

DAFTAR PUSTAKA

- Chengel. (n.d.). *fluid mechanic*. <https://www.ptonline.com/articles/how-to-get-better-mfi-results>
- D'ambros, A., Kipouros, T., Zachos, P., Savill, M., & Benini, E. (2018). Computational design optimization for S-Ducts. *Designs*, 2(4), 1–21. <https://doi.org/10.3390/designs2040036>
- Fox, R. W., McDonald, A. T., & Pritchard, P. J. (2011). *Introduction of Fluid Mechanics (8th ed.)*.
- Ghurri, A. (2014). Dasar-Dasar Mekanika Fluida. *Dasar-Dasar Mekanika Fluida*, 1. https://simdos.unud.ac.id/uploads/file_pendidikan_1_dir/2e54aeb12421ee1a17c35e14ba49cb23.pdf
- Leclercq, L., & Nardello-Rataj, V. (2020). How to improve the chemical disinfection of contaminated surfaces by viruses, bacteria and fungus? *European Journal of Pharmaceutical Sciences*, 155(August), 105559. <https://doi.org/10.1016/j.ejps.2020.105559>
- Malanichev, I., & Akhmadiev, F. (2020). Pressure loss reduction in ventilation ducts by shape optimization of the removable profiled components. *IOP Conference Series: Materials Science and Engineering*, 890(1). <https://doi.org/10.1088/1757-899X/890/1/012154>
- Manuel, M. C. E., Lin, P. T., & Chang, M. (2018). Optimal duct layout for HVAC using topology optimization. *Science and Technology for the Built Environment*, 24(3), 212–219. <https://doi.org/10.1080/23744731.2017.1346444>
- Perumal, K., & Ganesan, R. (2016). CFD modeling for the estimation of Pressure loss coefficients of pipe fittings: An undergraduate project. *Computer Applications in Engineering Education*, 24(2), 180–185. <https://doi.org/10.1002/cae.21695>
- Raber, E., Jin, A., Noonan, K., McGuire, R., & Kirvel, R. D. (2001). Decontamination issues for chemical and biological warfare agents: How clean is clean enough? *International Journal of Environmental Health*

- Research*, 11(2), 128–148. <https://doi.org/10.1080/09603120020047519>
- Reed, N. G. (2010). The history of ultraviolet germicidal irradiation for air disinfection. *Public Health Reports*, 125(1), 15–27. <https://doi.org/10.1177/003335491012500105>
- Röhrig, R., Jakirlić, S., & Tropea, C. (2015). Comparative computational study of turbulent flow in a 90° pipe elbow. *International Journal of Heat and Fluid Flow*, 55, 120–131. <https://doi.org/10.1016/j.ijheatfluidflow.2015.07.011>
- Salehi, M., Sleiti, A. K., & Idem, S. (2017). Study to identify computational fluid dynamics models for use in determining HVAC duct fitting loss coefficients. *Science and Technology for the Built Environment*, 23(1), 181–191. <https://doi.org/10.1080/23744731.2016.1204889>
- Sleiti, A., Salehi, M., & Idem, S. (2017). Detailed velocity profiles in close-coupled elbows—Measurements and computational fluid dynamics predictions (RP-1682). *Science and Technology for the Built Environment*, 23(8), 1212–1223. <https://doi.org/10.1080/23744731.2017.1285176>
- Smith, R. D. (2006). Responding to global infectious disease outbreaks: Lessons from SARS on the role of risk perception, communication and management. *Social Science and Medicine*, 63(12), 3113–3123. <https://doi.org/10.1016/j.socscimed.2006.08.004>
- Snelling, W. J., Afkhami, A., Turkington, H. L., Carlisle, C., Cosby, S. L., Hamilton, J. W. J., Ternan, N. G., & Dunlop, P. S. M. (2022). Efficacy of single pass UVC air treatment for the inactivation of coronavirus, MS2 coliphage and *Staphylococcus aureus* bioaerosols. *Journal of Aerosol Science*, 164(February), 106003. <https://doi.org/10.1016/j.jaerosci.2022.106003>
- Wang, M. D., & Jolly, A. M. (2004). Changing virulence of the SARS virus: The epidemiological evidence. *Bulletin of the World Health Organization*, 82(7), 547–548.
- Wang, Z., Qiang, W., & Ke, H. (2020). A Handbook of 2019-nCoV Pneumonia Control and Prevention. *Hubei Science and Technology Press*, 1–108.
- Wojewodka, M. M., White, C., Shahpar, S., & Kontis, K. (2018). A review of flow control techniques and optimisation in s-shaped ducts. *International Journal of Heat and Fluid Flow*, 74(June), 223–235.

<https://doi.org/10.1016/j.ijheatfluidflow.2018.06.016>

Yang, Y., Lai, A. C. K., Kong, R. Y. C., & Deng, Q. (2017). Experimental and numerical study of the performance of upper-room ultraviolet germicidal irradiation with the effective Z-value of airborne bacteria. *Aerosol Science and Technology*, *51*(10), 1123–1134.

<https://doi.org/10.1080/02786826.2017.1334108>

Zhang, H., Jin, X., Nunayon, S. S., & Lai, A. C. K. (2020). Disinfection by in-duct ultraviolet lamps under different environmental conditions in turbulent airflows. *Indoor Air*, *30*(3), 500–511. <https://doi.org/10.1111/ina.12642>

LAMPIRAN

Lampiran 1. Tabel Data Penelitian

Tabel 6 Data penelitian pada pengujian eksperimental

Variasi jumlah sekat (N)	Daya (Volt)	Δh Dinamis (m)	h Statis <i>Inlet</i> (m)	h Statis <i>Outlet</i> (m)
0	100	0,009	0,012	0,0008
	130	0,013	0,018	0,001
	160	0,017	0,024	0,0015
	190	0,021	0,028	0,0018
	220	0,023	0,032	0,002
2	100	0,008	0,012	0,0008
	130	0,012	0,018	0,001
	160	0,016	0,024	0,0015
	190	0,02	0,03	0,0018
	220	0,022	0,032	0,002
4	100	0,007	0,012	0,0008
	130	0,011	0,018	0,001
	160	0,015	0,024	0,0013
	190	0,017	0,028	0,0015
	220	0,019	0,032	0,0018
6	100	0,006	0,012	0,0005
	130	0,01	0,02	0,0008
	160	0,014	0,028	0,001
	190	0,016	0,032	0,0013
	220	0,018	0,036	0,0015

Tabel 7 Data Hasil Perhitungan pada pengujian eksperimental

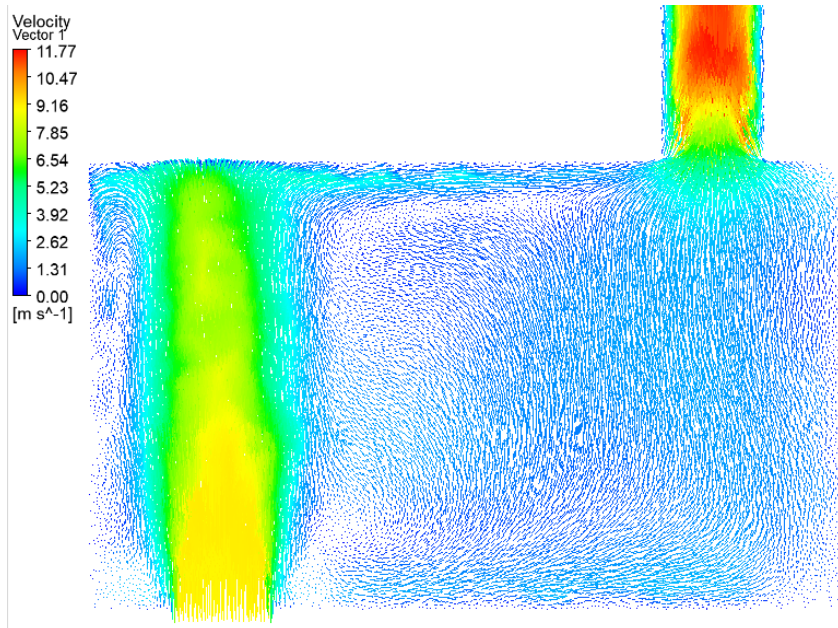
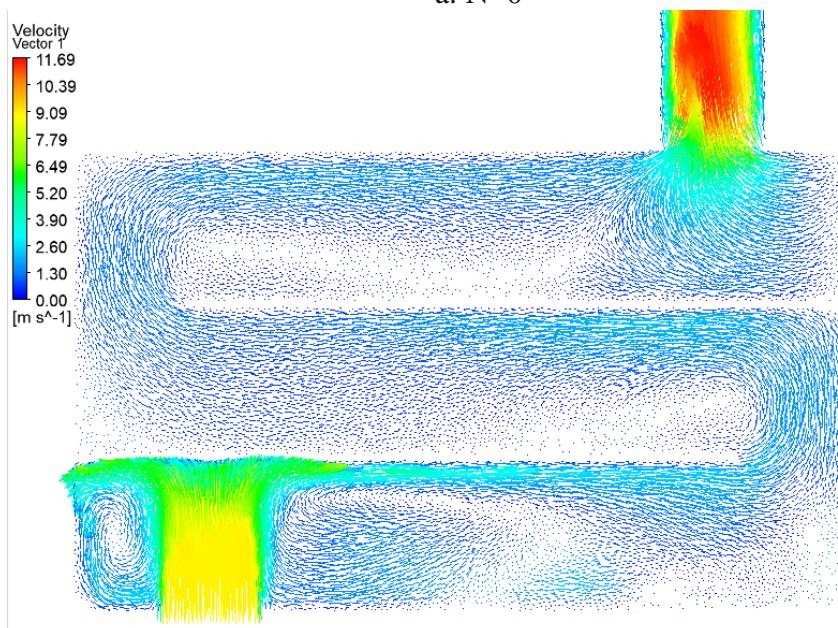
Variasi jumlah sekat (N)	Daya (Volt)	Eksperimenteal			
		V (m/s)	P in (Pa)	P out (Pa)	ΔP (Pa)
0	100	8,23	63,08	4,21	58,87
	130	9,89	94,62	5,26	89,36
	160	11,31	126,16	7,89	118,28
	190	12,57	147,19	9,46	137,73
	220	13,16	168,21	10,51	157,70
2	100	7,76	63,08	4,21	58,87
	130	9,50	94,62	5,26	89,36
	160	10,97	126,16	7,89	118,28
	190	12,27	157,70	9,46	148,24
	220	12,87	168,21	10,51	157,70
4	100	7,26	63,08	4,21	58,87
	130	9,10	94,62	5,26	89,36
	160	10,62	126,16	6,83	119,33
	190	11,31	147,19	7,89	139,30
	220	11,96	168,21	9,46	158,75
6	100	6,72	63,08	2,63	60,45
	130	8,67	105,13	4,21	100,93
	160	10,26	147,19	5,26	141,93
	190	10,97	168,21	6,83	161,38
	220	11,64	189,24	7,89	181,36

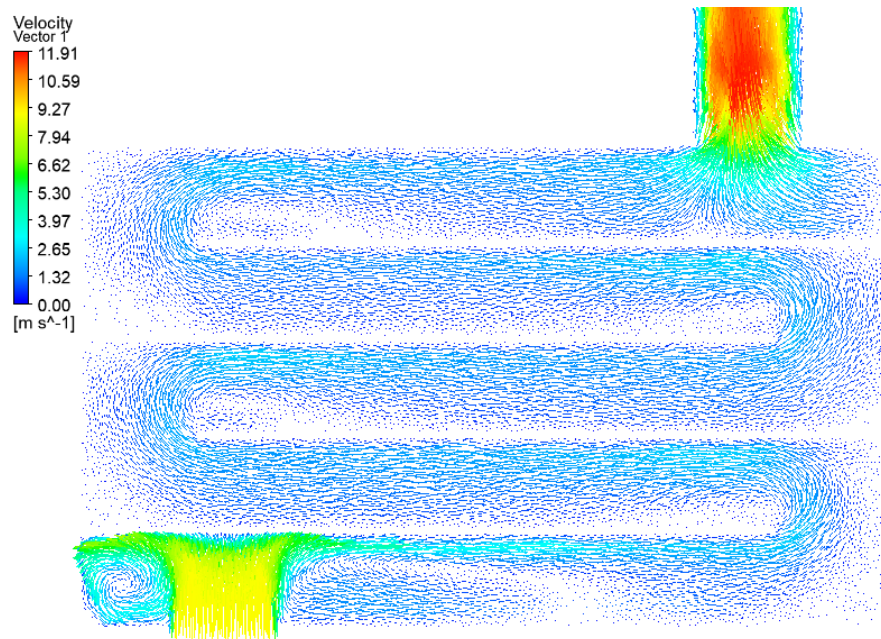
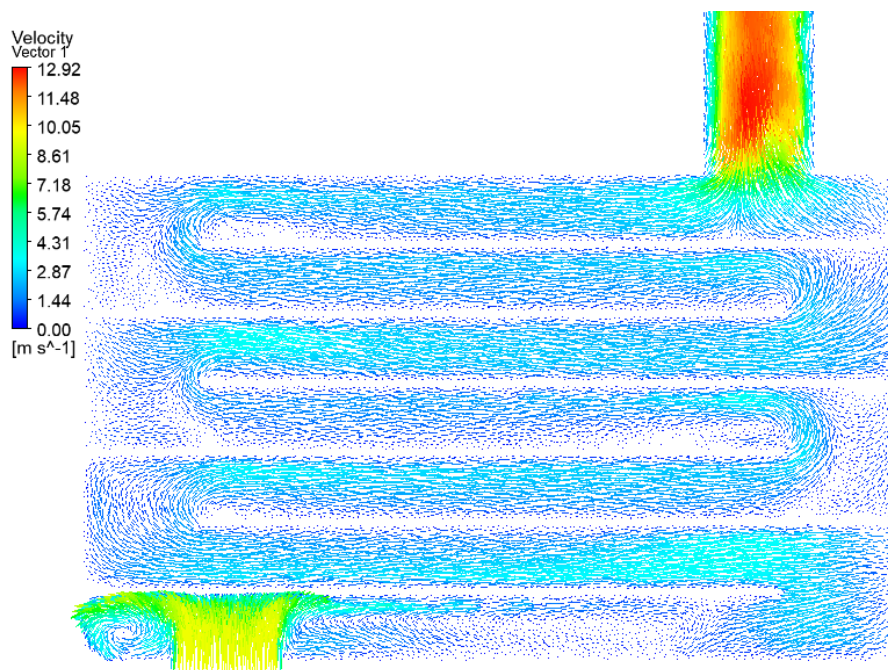
Tabel 8 Data hasil perhitungan pada pengujian komputasi

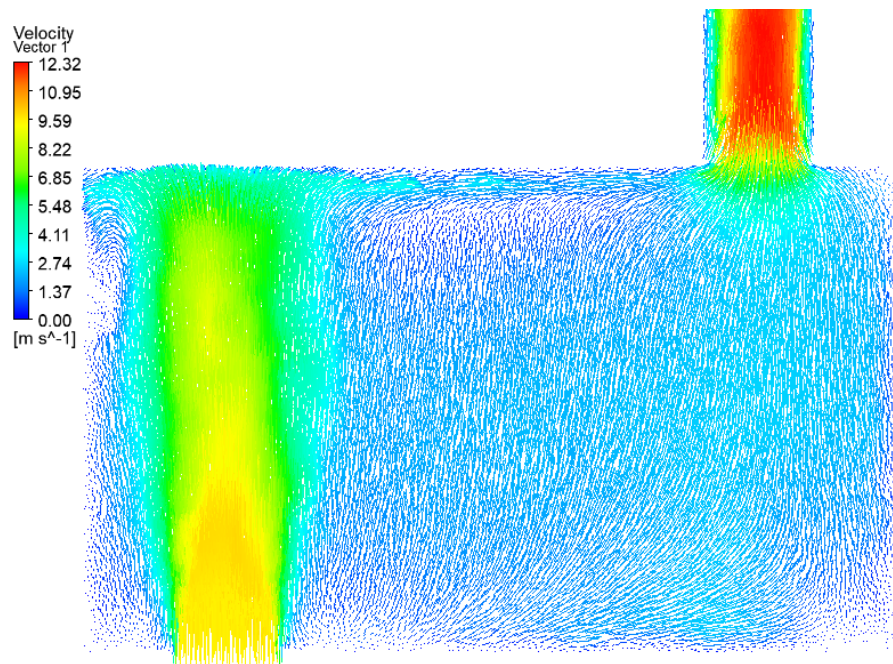
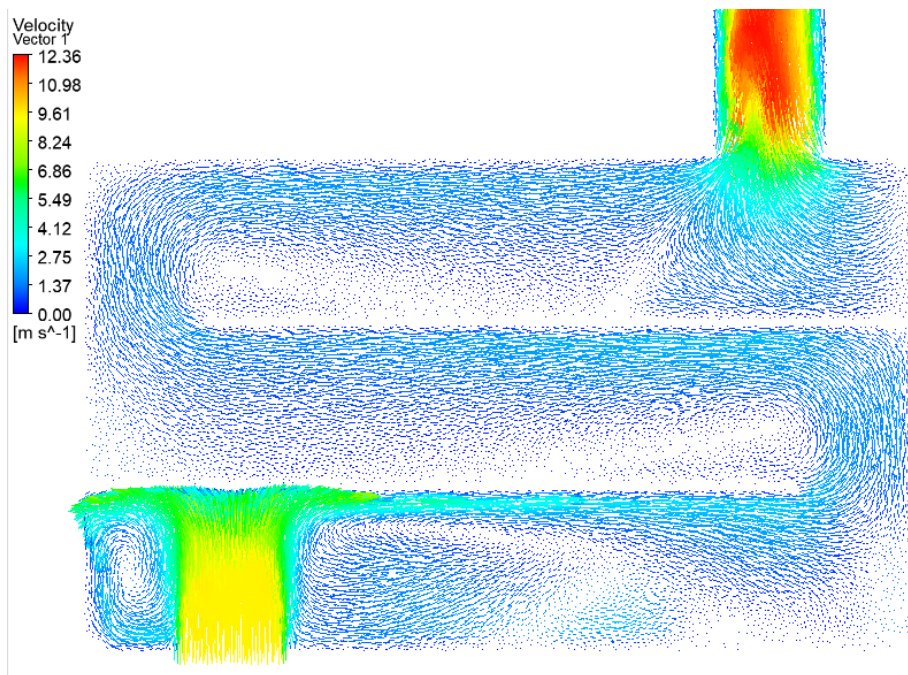
Variasi jumlah sekat (N)	Komputasi			
	V (m/s)	P in (Pa)	P out (Pa)	ΔP (Pa)
0	8,23	69,67	5,25	64,42
	9,89	104,87	7,99	96,88
	11,31	138,75	9,32	129,43
	12,57	163,67	13,11	150,56
	13,16	183,88	11,60	172,29
2	7,76	68,47	5,71	62,76
	9,50	101,75	8,15	93,60
	10,97	135,33	10,56	124,77
	12,27	168,23	12,92	155,31
	12,87	184,80	12,97	171,83
4	7,26	64,25	4,67	59,58
	9,10	101,09	7,00	94,08
	10,62	135,20	8,48	126,72
	11,31	153,23	9,30	143,94
	11,96	181,48	10,35	171,13
6	6,72	69,10	3,90	65,20
	8,67	113,30	3,65	109,65
	10,26	160,77	7,08	153,68
	10,97	182,86	7,19	175,67
	11,64	206,36	8,01	198,35

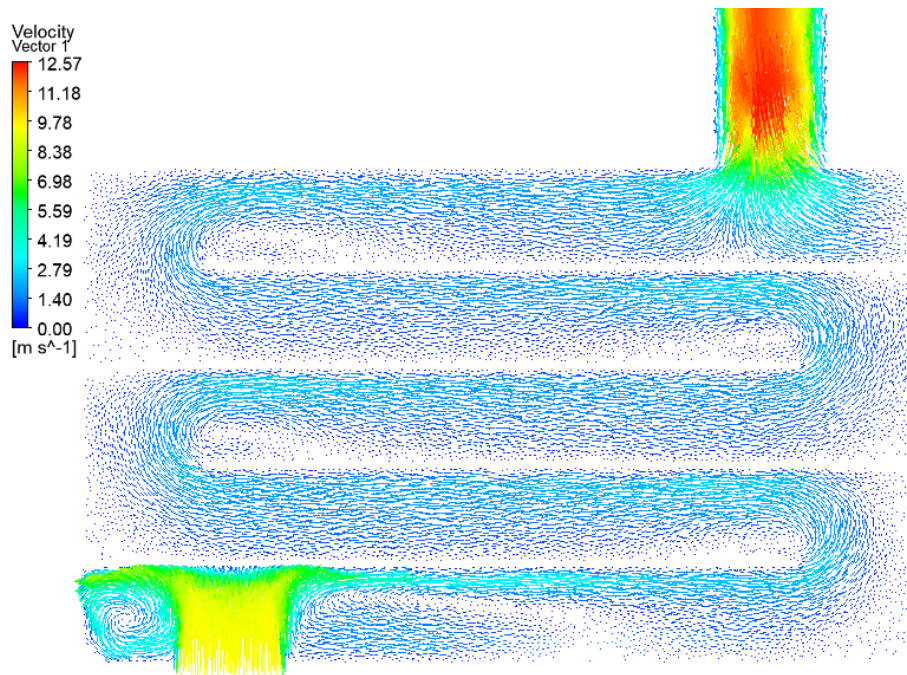
Tabel 9 Data selisih perbandingan pengujian eksperimental dan komputasi

Variasi jumlah sekat (N)	Daya (Volt)	V (m/s)	Eksperimenteal	Komputasi	Selisih (%)
			ΔP (Pa)	ΔP (Pa)	
0	100	8,23	58,87	64,42	9%
	130	9,89	89,36	96,88	8%
	160	11,31	118,28	129,43	9%
	190	12,57	137,73	150,56	9%
	220	13,16	157,70	172,29	9%
2	100	7,76	58,87	62,76	7%
	130	9,50	89,36	93,60	5%
	160	10,97	118,28	124,77	5%
	190	12,27	148,24	155,31	5%
	220	12,87	157,70	171,83	9%
4	100	7,26	58,87	59,58	1%
	130	9,10	89,36	94,08	5%
	160	10,62	119,33	126,72	6%
	190	11,31	139,30	143,94	3%
	220	11,96	158,75	171,13	8%
6	100	6,72	60,45	65,20	8%
	130	8,67	100,93	109,65	9%
	160	10,26	141,93	153,68	8%
	190	10,97	161,38	175,67	9%
	220	11,64	181,36	198,35	9%

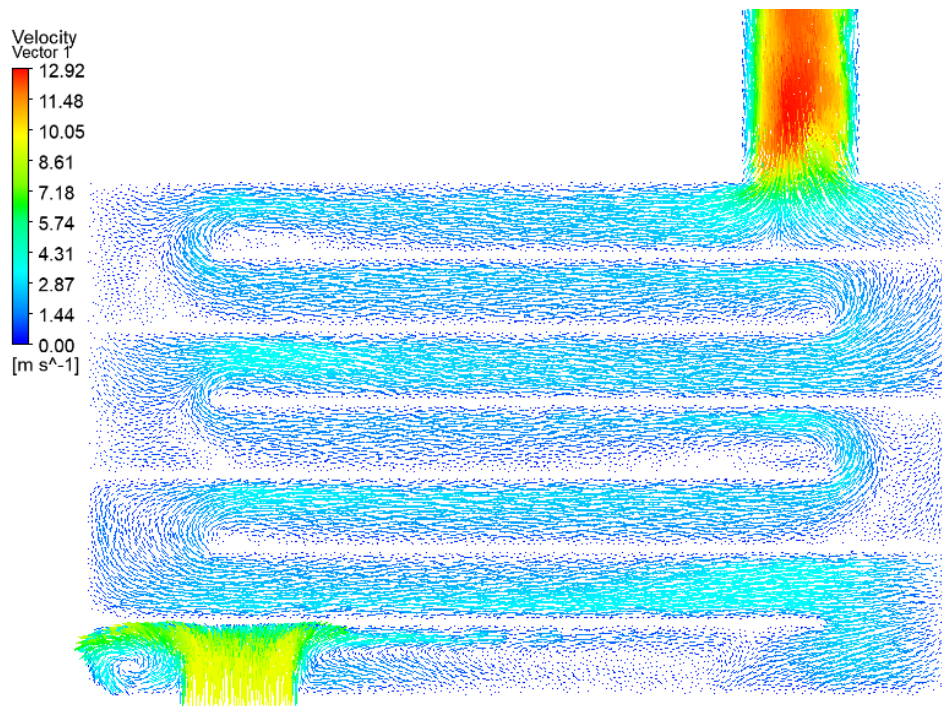
Lampiran 2. Profil Kecepatan pada $v_{inlet} = 9$ m/s, 9.5 m/s, dan 10 m/sa. $N=0$ b. $N=2$

c. $N=4$ d. $N=6$ Gambar 26 Vektor kecepatan pada $v_{inlet} = 9$ m/s

a. $N=0$ b. $N=2$

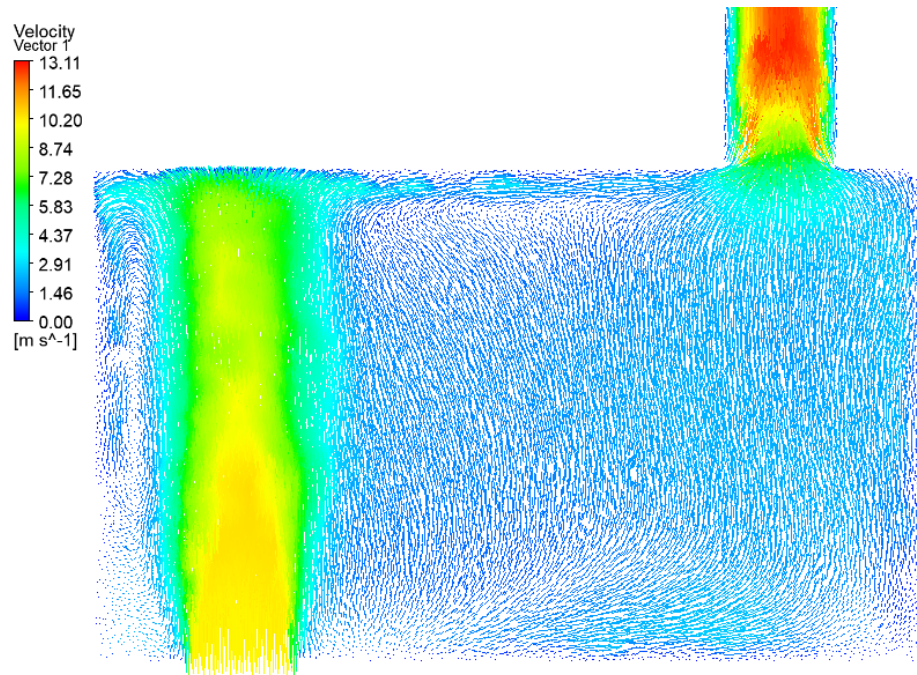
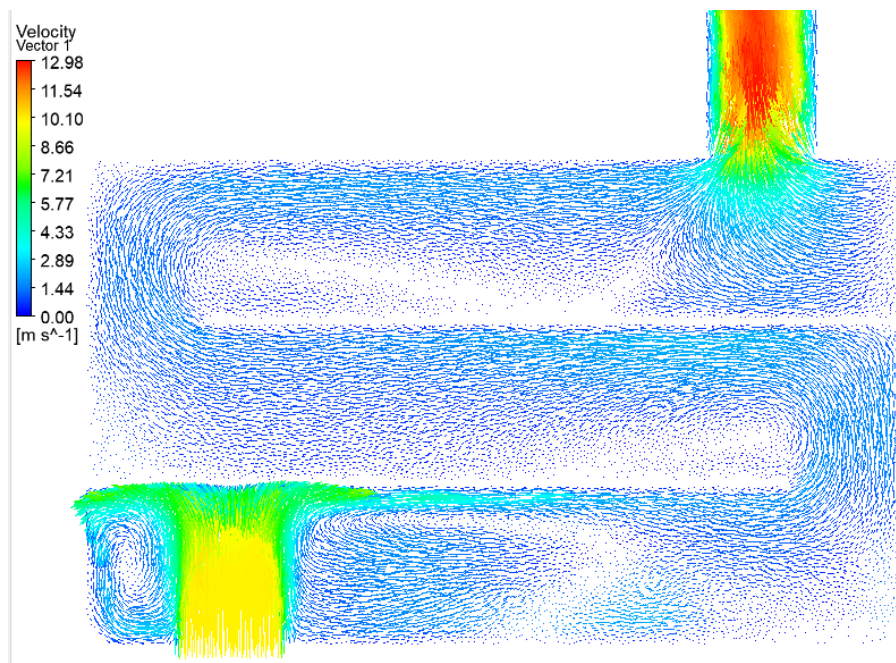


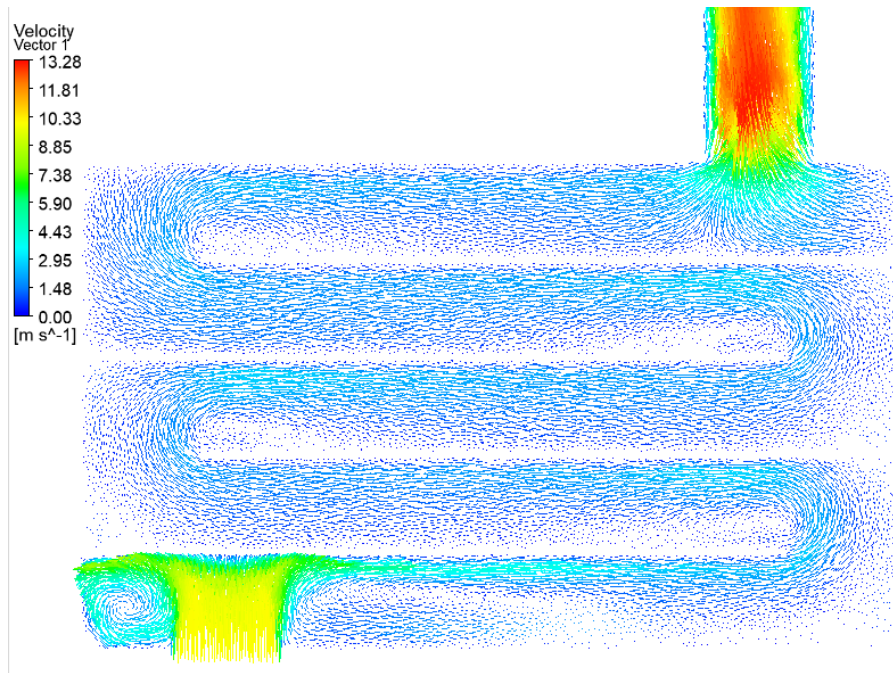
c. N=4



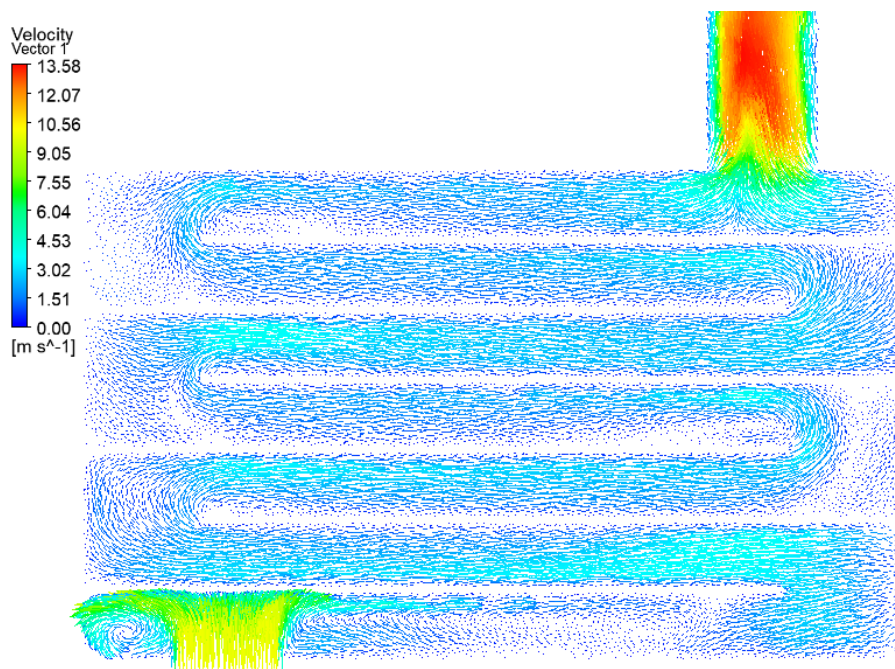
d. N=6

Gambar 27 Vektor kecepatan pada $v_{inlet} = 9,5$ m/s

a. $N=0$ b. $N=2$



c. N=4



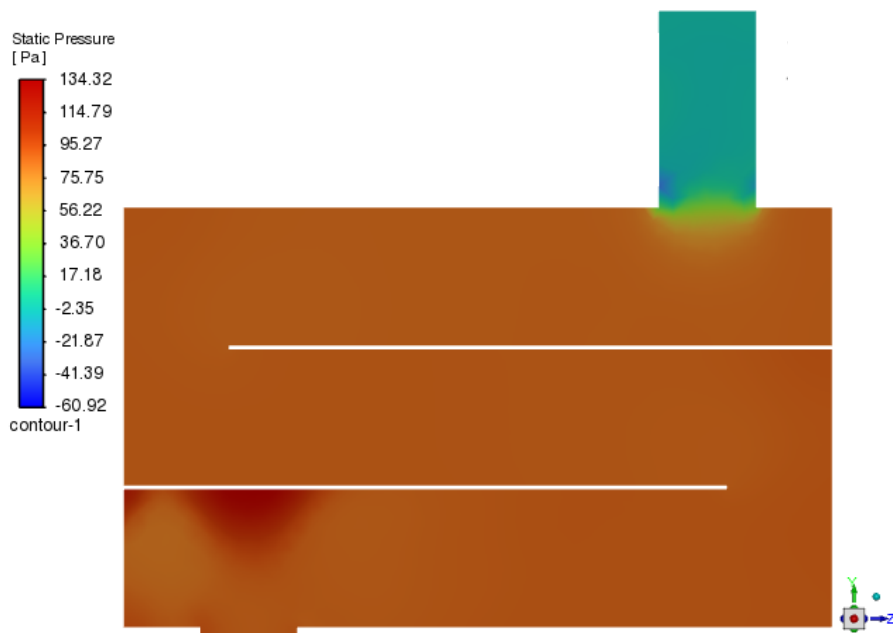
d. N=6

Gambar 28 Vektor kecepatan pada $v_{inlet} = 10$ m/s

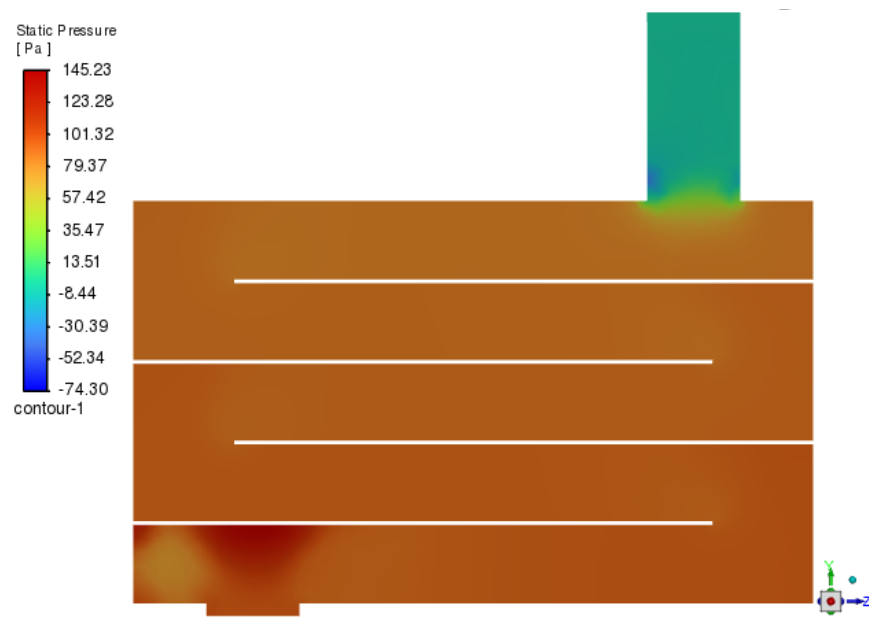
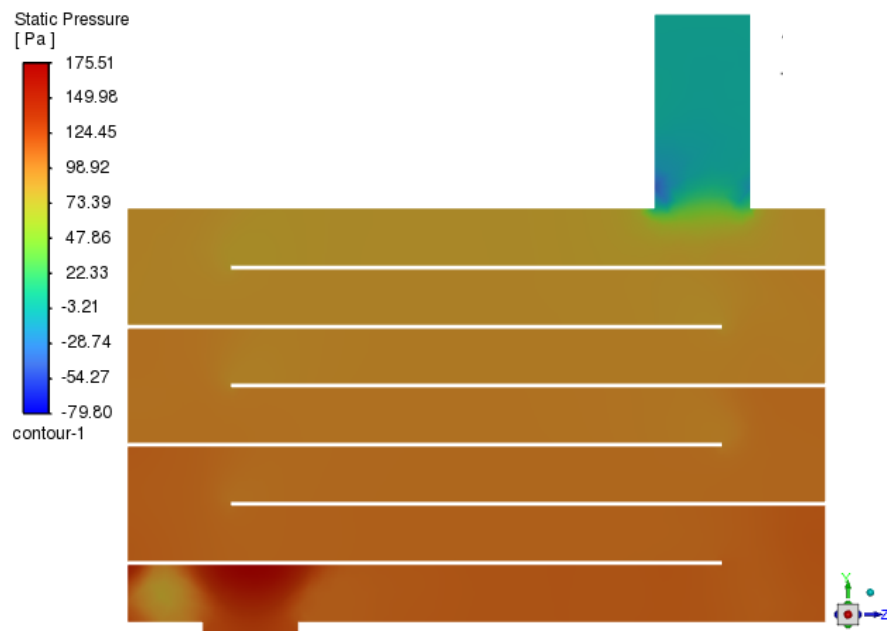
Lampiran 3. Profil tekanan pada $v_{inlet} = 9$ m/s, 9.5 m/s, dan 10 m/s.

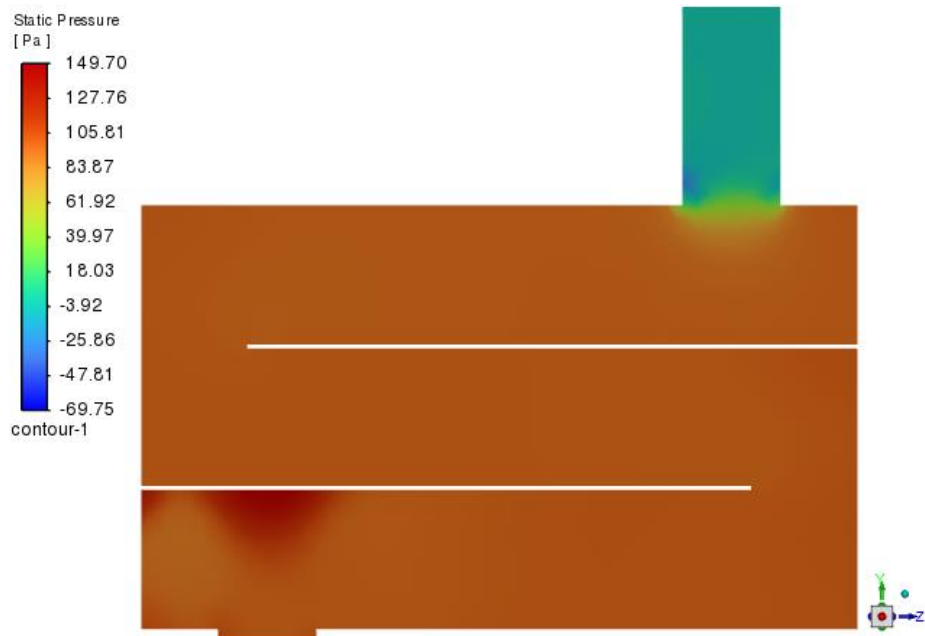


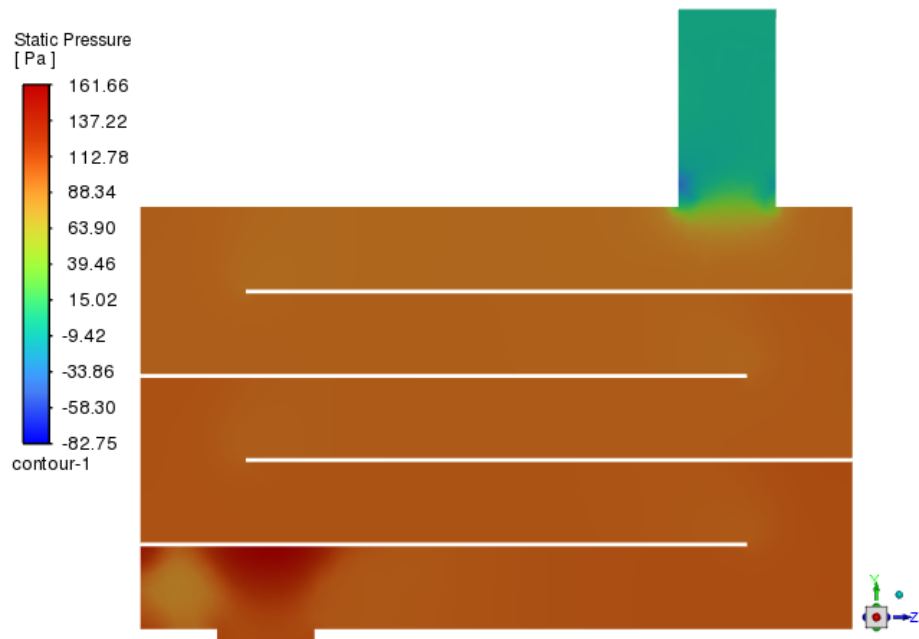
a. $N=0$



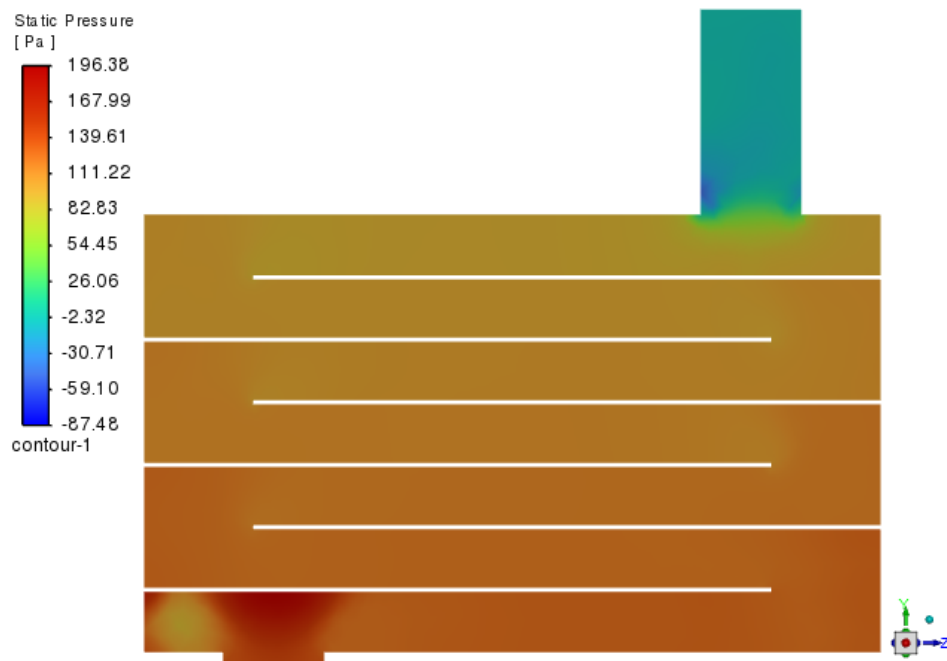
b. $N=2$

c. $N=4$ d. $N=6$ Gambar 29 Kontur tekanan pada $v_{inlet} = 9 \text{ m/s}$

a. $N=0$ b. $N=2$

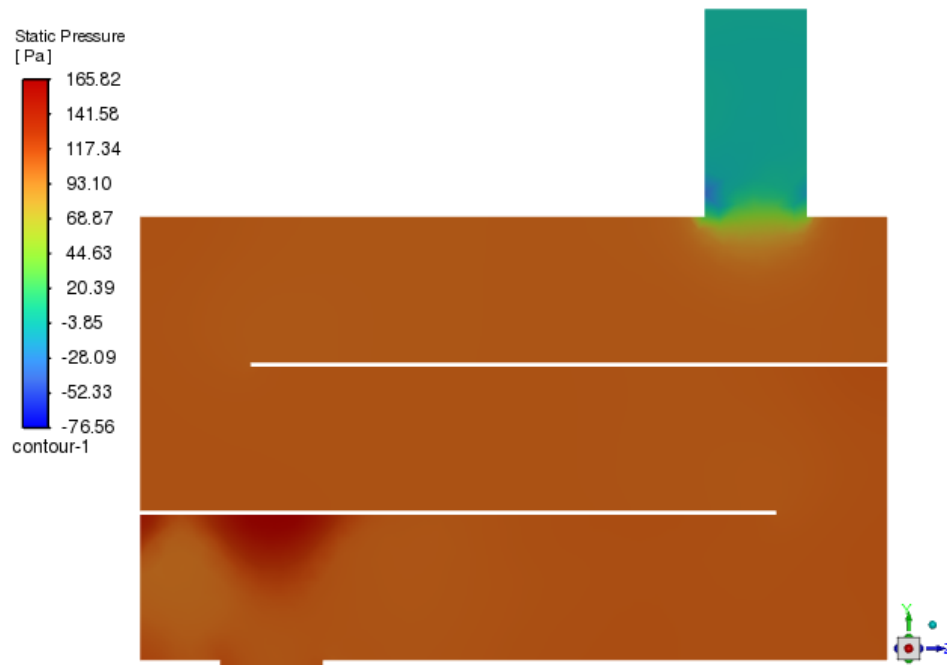


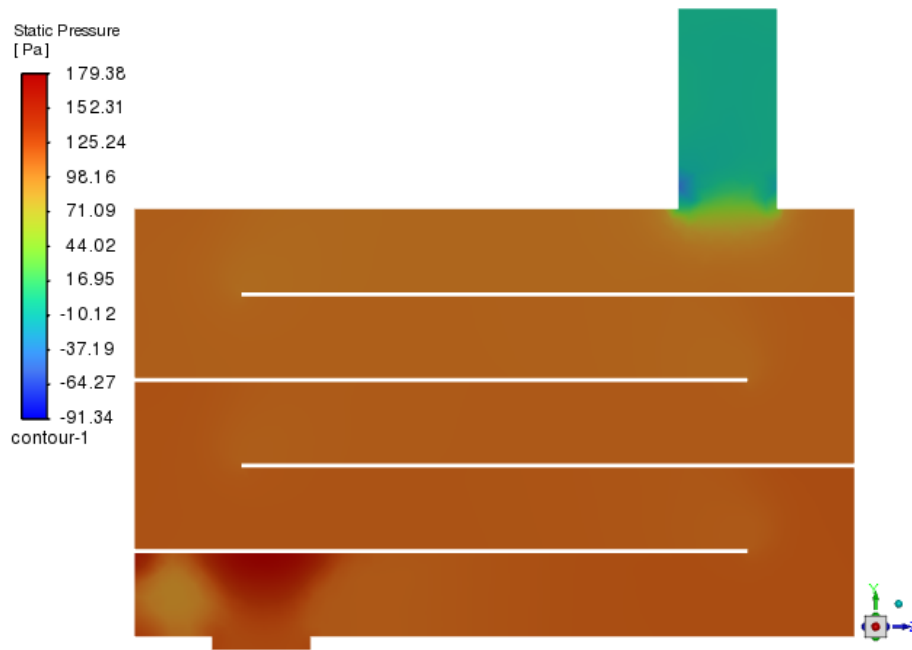
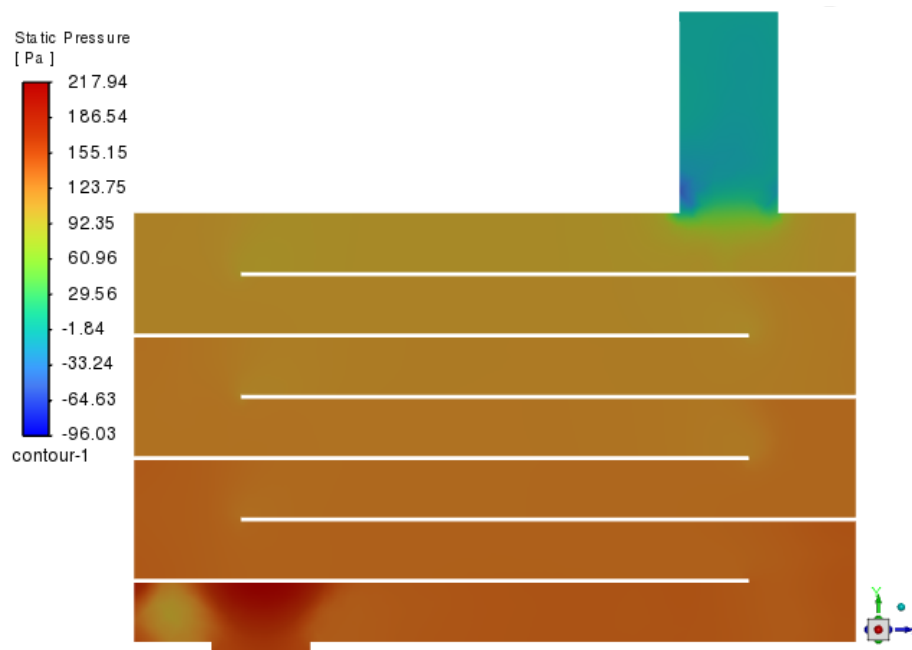
c. N=4



d. N=6

Gambar 30 Kontur tekanan pada $v_{inlet} = 9,5$ m/s

a. $N=0$ b. $N=2$

c. $N=4$ d. $N=6$ Gambar 31 Kontur tekanan pada $v_{inlet} = 10$ m/s.

Lampiran 4. Dokumentasi Penelitian



Gambar 32 Proses perakitan alat



Gambar 33 Proses pengambilan data Eksperimen

Lampiran 5. Jurnal

KARAKTERISTIK ALIRAN FLUIDA PADA CHAMBER MOBILE ROBOT DISINFEKTAN MENGGUNAKAN ULTRAVIOLET C (UVC)

Moh. Fajri Sidik,¹ Nasaruddin Salam² & Andi Amijoyo Mochtar³

¹*Department of Mechanical Engineering, Gowa, Hasanuddin University, Indonesia*

²*Department of Mechanical Engineering, Gowa, Hasanuddin University, Indonesia*

³*Department of Mechanical Engineering, Gowa, Hasanuddin University, Indonesia*

*Address all correspondence to: First A. Author, Business or Academic Affiliation 1, City, State, Zip Code, E-mail: f.author@affiliation.com

*Original Manuscript Submitted: mm/dd/yyyy; Final Draft
Received: mm/dd/yyyy*

Air purification systems using ultraviolet light C (UVC) are increasingly being used to produce good air quality, the chamber in the air purification device plays an important role in the disinfection process. By providing a bulkhead in the chamber, it can increase the UV exposure time to the air so that it effectively inactivates bioaerosols containing bacterial and viral organisms, as well as corona viruses without relying on filtration technology. This study aims to determine the effect of the number of bulkheads in the chamber on fluid flow characteristics and the Pressure drop that occurs at the inlet and outlet of the disinfectant mobile robot chamber. Speed and Pressure tests were carried out at centrifugal blower voltages of 100 to 220 volts. The results obtained from the experiment show that the more the number of bulkheads the air velocity in the chamber decreases and the Pressure drop that occurs increases.

KEY WORDS: *Karakteristik aliran, Penurunan tekanan, Chamber, CFD FLUENT*

1.INTRODUCTION

Harmful microorganisms suspended in the air or attached to surfaces are a major threat to human health (M. D. Wang and Jolly 2004). Before the outbreak of the deadly coronavirus in 2020, there have been several cases reported in the past such as, severe acute respiratory syndrome (SARS) in 2003 and H1N1 in 2010 (Smith 2006).

The coronavirus can spread through various ways, humans are one of the main sources of virus transmission through droplets or particles caused by coughing or sneezing. In addition, other media such as metal, paper, and glass can also be a place where the coronavirus spreads. However, because the coronavirus is sensitive to heat, disinfectants containing chlorine and fat solvents at 56oC for 30 minutes, ether, alcohol, peracetic acid, formalin, oxidants and chloroform can kill the coronavirus (Z. Wang, Qiang, and Ke 2020).

Chemical methods are the most commonly used to remove harmful microorganisms (Leclercq and Nardello-Rataj 2020). There are some major drawbacks when using chemicals in this way. Chemicals can selectively kill microorganisms; they take time to completely kill microorganisms (in some cases up to 1 hour). Unreacted chemical compounds can contaminate the environment and

the cleaning process is usually limited to surfaces, being less effective when used against airborne microorganisms (Raber et al. 2001).

One of the most effective methods to disinfect air from pathogens is to use ultraviolet C radiation (UVC, wavelength 200-280 nm) has been shown to inactivate microorganisms by damaging the nucleic acids and proteins of pathogens, which causes the malfunction of the pathogen's reproductive process and leads to cell death (Reed 2010; Yang et al. 2017). In (Zhang et al. 2020) by investigating the effect of environmental factors such as airflow velocity, relative humidity (RH), temperature and channel reflectance on the performance of UVC lamps in the channel. *Staphylococcus epidermidis*, *Pseudomonas alcaligenes* and *Escherichia coli* were used as bacterial tests. The UV irradiance, disinfection efficacy, and UV susceptibility constant (Z value) of the test bacteria were experimentally determined. The results showed that the UV disinfection efficacy decreased as the airflow velocity and RH increased.

In research (Snelling et al. 2022) with a portable UVC air treatment device with the use of 3 bulkheads in the UV *chamber* with an air flow of 1254 L / min can increase exposure time so as to effectively inactivate bioaerosols containing bacterial and viral indicator organisms, as well as coronaviruses without relying on filtration technology.

However, the addition of bulkheads can also affect fluid flow and *Pressure* drop in the UV *chamber*. *Pressure* drop is one of the influential ones in improving energy utilisation, saving energy, and reducing emissions. Experimental and numerical research using CFD to can be conducted for the prediction of *Pressure* drop in line fittings and the factors affecting its accuracy (Perumal and Ganesan 2016; Röhrig, Jakirlić, and Tropea 2015; Salehi, Sleiti, and Idem 2017; Sleiti, Salehi, and Idem 2017; Malanichev and Akhmadiev 2020). It was found that the combination of the k- ϵ model and a high-order discrete numerical scheme resulted in a high degree of accuracy (with a relative error of 10%).

Numerous studies have been conducted to understand localised *Pressure* losses in ducts and pipes and optimise new and existing system components (Wojewodka et al. 2018; Manuel, Lin, and Chang 2018; D'ambros et al. 2018). *Pressure* drop in the duct can result from localised resistance at intervening elements such as bends, branches, fittings due to flow adjustment and deformation, formation of *vortex* flow when flow is stalled from sharp edges of structures, occurrence of circulation zones, sharp surface intervening elements.

Seeing the lack of published literature related to fluid flow and *Pressure* drop in the UV *chamber*, it is necessary to conduct further research to determine the fluid flow characteristics in the UV *chamber* with the addition of variations in the number of bulkheads and their effect on *Pressure* drop.

1. METHODOLOGY

2.1 Chamber design of mobile robot UV disinfectant

The 3D *chamber* model was designed using Solidworks 2020, the finished model was then transferred to Ansys® Fluent fluid simulation software to perform the simulation. The purpose of the simulation is to determine the fluid flow characteristics and *Pressure* drop in the *chamber*. *Chamber* dimensions used are 54 cm long, 54 cm wide, and 32 cm high as shown in Figure 1.

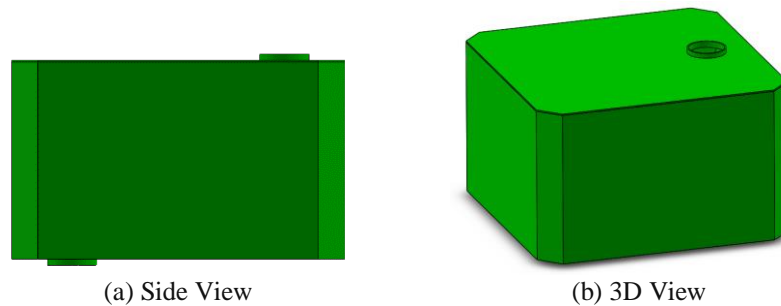


FIG. 1: Chamber Mobile robot UV disinfectan

The inside of the *chamber* is given a bulkhead with a variation in the number of bulkheads (N) of 0, 2, 4, 6 as shown in Figure 2, Model (a) is a *chamber* without the addition of bulkheads ($N=0$), model (b) added 2 bulkheads with a distance between bulkheads of 103 mm ($N=2$), in model (c) added 4 bulkheads with a distance between bulkheads of 65 mm ($N=4$), and in model (d) added 6 bulkheads with a distance between bulkheads of 52 mm ($N=6$).

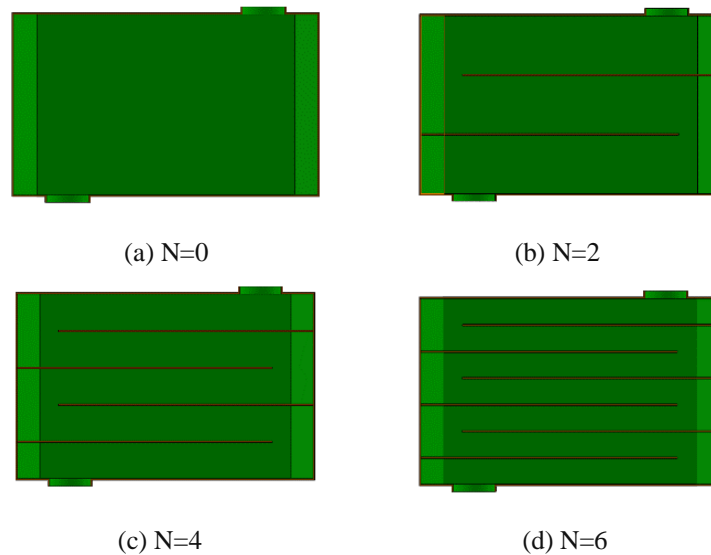


FIG. 2: Chamber bulkheads

2.2 Meshing CFD

To capture the three-dimensional flow inside the domain with reasonable accuracy, a good quality mesh is required. An unstructured tetrahedral mesh is considered best for this case.

2.3 Boundary Condition

In the *Chamber* design, the *outlet chamber* design is extended to make the results more accurate. The amount of air entering the *inlet* is determined and set as the *inlet* boundary condition. The *Chamber outlet* boundary condition is defined as the *outlet Pressure*, while the wall is set as a smooth wall. In this way, CFD analysis can be used to easily calculate the *Pressure* loss between the *inlet* and *outlet* of the *chamber*. The analysis is performed under steady state. The *chamber inlet* is defined as the flow velocity and the *outlet* is defined as the *outlet Pressure*.

2.4 Governing equations

The Ansys Fluent commercial CFD solver used for this study is a finite volume approach-based solver that is widely used in industry. The equations solved with the software, for this study in Cartesian form are as follows:

Continuity :

$$\frac{\partial \rho}{\partial t} + \text{div} (\rho u) = 0 \quad (1)$$

$\frac{\partial \rho}{\partial t}$ = Density flow rate over time

$\text{div} (\rho u)$ = Net flow of mass leaving an element across its boundary.

Momentum:

According to Newton's law, the rate of change of momentum of a fluid particle is equal to the sum of the forces acting on the particle. Using this, the momentum equation of the X component is given as,

$$\rho \frac{Du}{Dt} = \frac{\partial(-P+\tau_{xx})}{\partial x} + \frac{\partial\tau_{yx}}{\partial y} + \frac{\partial\tau_{zx}}{\partial z} + S_{Mx} \quad (2)$$

Similarly, the components of the momentum equation Y are,

$$\rho \frac{Du}{Dt} = \frac{\partial\tau_{xy}}{\partial x} + \frac{\partial(-P+\tau_{yy})}{\partial y} + \frac{\partial\tau_{zy}}{\partial z} + S_{My} \quad (3)$$

And the components of the momentum equation Z are,

$$\rho \frac{Du}{Dt} = \frac{\partial\tau_{xz}}{\partial x} + \frac{\partial\tau_{yz}}{\partial y} + \frac{\partial(-P+\tau_{zz})}{\partial z} + S_{Mz} \quad (4)$$

Where ρ is density, P is *Pressure*, $\tau(x,y,z)$ is shears stress in the x,y,z direction, $SM(x,y,z)$ is the source of momentum per unit volume per unit time in the x,y,z direction.

Model Turbulensi:

The standard turbulence model ($k-\epsilon$) is used over other turbulence models because it can predict the boundary layer under strong adverse *Pressure* gradients or separation. Rotational and recirculating flows can be modelled appropriately using this model. Standard ($k-\epsilon$) turbulence uses two partial differential equations to estimate the velocity and length scales and is therefore commonly known as the two-equation turbulence model.

Inlet Condition:

Velocity = 8,5 m/s

Outlet Condition:

Pressure = atmospheric *Pressure*

Air properties:

Density = 1.11 kg/m³

Vicosity = 1.94 x 10⁻⁵ kg/m^s

2. RESULTS AND DISCUSSION

Figure 3 shows the location of the AA section where the Velocity and *Pressure* contours were plotted at each bulkhead number.

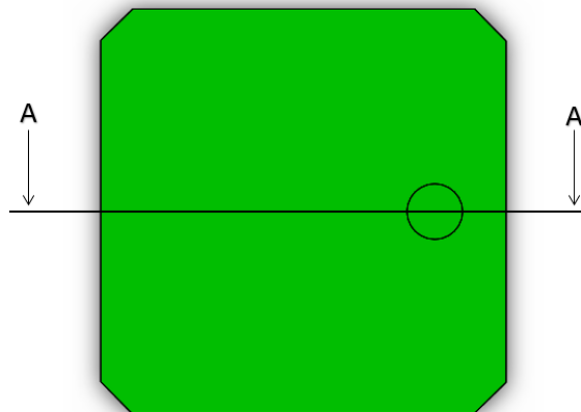


FIG. 3: Location of the AA section

3.1 Profil kecepatan

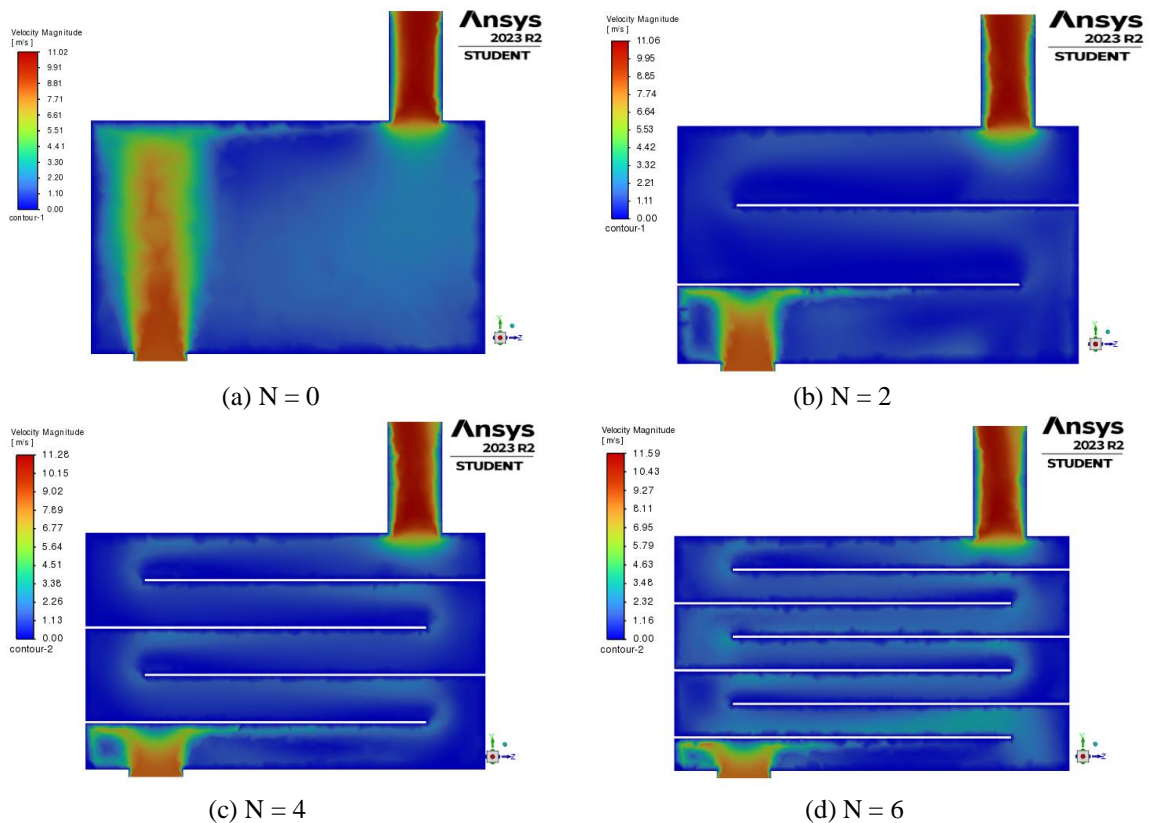


FIG. 4: velocity contour of the AA section

In Figure 4 it can be seen that there is a significant difference in each bulkhead variation, in the $N = 0$ variation the fluid flow entering the *chamber* goes directly to the top surface of the *chamber* then spreads in various directions before finally exiting at the *outlet*. At variations $N = 2$, $N = 4$, and $N = 6$ it can be seen that the movement of fluid flow is more regular following the pattern of each bulkhead variation and with the use of bulkheads in the *chamber* resulting in *swirl / vortex*, *swirl / vortex* occurs due to the turning of fluid flow in the *chamber*. Increasing the number of bulkheads causes an increase in turns in the *chamber* but the *swirl/vortex* area at each turn is getting smaller this is caused by the decreasing distance between the bulkheads.

At the *outlet* of the *chamber*, it can be seen that the velocity increases in the middle of the *outlet* can be seen in red in the middle and blue at the edge of the *outlet*, this is due to the venturi effect due to changes in the viewing area when entering the *outlet*.

3.2 Pressure Profile

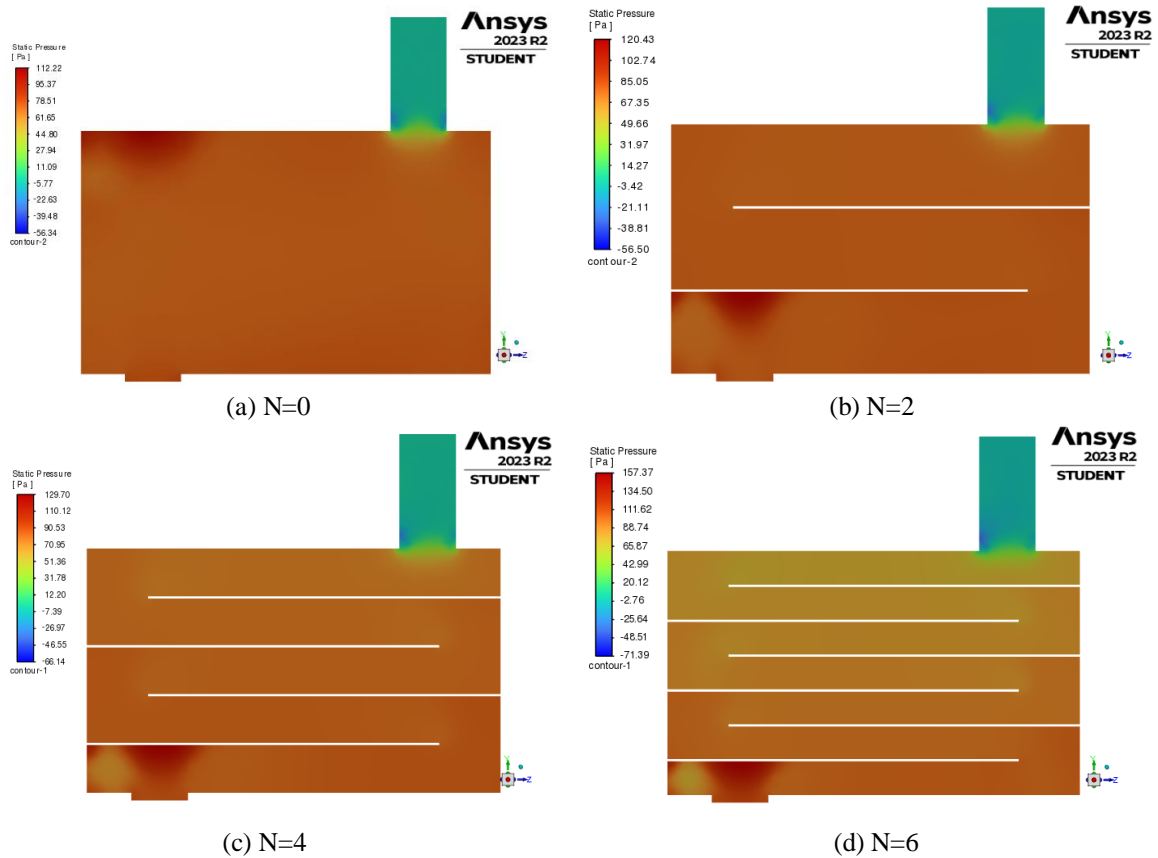


FIG.5: Pressure Contour in Section AA

From Figure 5, it can be seen that there is a decrease in *Pressure* at the *inlet* and *outlet* of the *chamber*, it can be seen from the red *inlet* section and the blue *outlet* section, this occurs in the *chamber* without bulkheads or with the addition of bulkheads, the *Pressure* drop occurs due to the difference in cross-sectional area in the *chamber* and the friction force on the surface of the *chamber* wall.

The highest *Pressure* area is in the part where the fluid flow crashes after entering the *chamber*, this occurs because the collision of the fluid flow in the area causes a sudden decrease in speed before finally spreading to an area with low *Pressure*. The lowest *Pressure* area is at the *outlet* of the *chamber*, the *Pressure* drop is caused by the venturi effect where a change in cross-sectional surface area occurs when entering the *outlet chamber*.

3.3 Pressure Drop

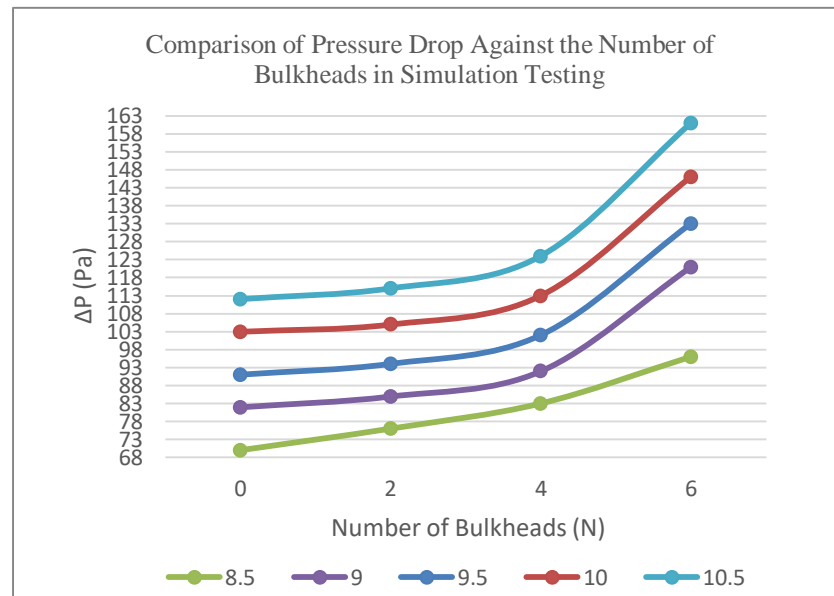


FIG. 6: Comparison chart of *Pressure* drop against the number of baffles

CFD analysis is performed with different velocities based on the applied voltage. The *Pressure* drop in the *chamber* is calculated by taking the average *Pressure* difference at the *inlet* and *outlet* of the *inlet* system. The CFD simulation shows the *Pressure* drop as shown in figure 5.

In Figure 6 it can be seen that at a speed of 8.5 m/s the *chamber* without bulkheads produces the lowest *Pressure* drop value with a value of 70 Pa, then increases with the addition of 2 bulkheads with a value of 76 Pa, 4 bulkheads with a value of 83 Pa, and the highest *Pressure* drop is in the *chamber* with the addition of 6 bulkheads with a value of 96 Pa. So, with the addition of bulkheads in the *chamber*, the value of the *Pressure* drop increases and the increase that occurs is getting higher as the number of bulkheads increases. It can also be seen that the *Pressure* drop that occurs increases with increasing speed where at a speed of 10.5 m/s the value of *Pressure* drop in the *chamber* without bulkhead 112 Pa, 2 bulkheads with a value of 115 Pa, 4 bulkheads with a value of 124 Pa, and at 6 bulkheads with a value of 161 Pa.

The increase in the amount of *Pressure* drop with the addition of bulkheads is due to the friction that occurs will increase and the increase in the number of turns resulting in an increase in the *swirl* / *vortex* that occurs in the *chamber*.

3. CONCLUSIONS

Computational analysis of fluid in the *chamber* of a *mobile* robot uv disinfectant is carried out to predict flow characteristics and *Pressure* drop. The application of the addition of bulkheads in the *chamber* makes the fluid flow distribution pattern more regular but makes the turns increase so that the *swirl* / *vortex* that occurs at each turn and the value of the *Pressure* drop at the *inlet* and *outlet* of the *chamber* increases along with the increase in the number of bulkheads, this is due to the friction area that occurs will increase and the increase in the number of turns resulting in an increase in *swirl* / *vortex* that occurs in the *chamber*.

ACKNOWLEDGEMENT

Institute for Research and Community Service (LPPM) Universitas Hasanuddin. Number : 1474/UN4.22/PT.01.03/2022.

REFERENCES

- D'ambros, Alessio, Timoleon Kipouros, Pavlos Zachos, Mark Savill, and Ernesto Benini. 2018. "Computational Design Optimization for S-Ducts." *Designs* 2 (4): 1–21. <https://doi.org/10.3390/designs2040036>.
- Leclercq, Loïc, and Véronique Nardello-Rataj. 2020. "How to Improve the Chemical Disinfection of Contaminated Surfaces by Viruses, Bacteria and Fungus?" *European Journal of Pharmaceutical Sciences* 155 (August): 105559. <https://doi.org/10.1016/j.ejps.2020.105559>.
- Malanichev, Igor, and Fail Akhmadiev. 2020. "Pressure Loss Reduction in Ventilation Ducts by Shape Optimization of the Removable Profiled Components." *IOP Conference Series: Materials Science and Engineering* 890 (1). <https://doi.org/10.1088/1757-899X/890/1/012154>.
- Manuel, Mark Christian E., Po Ting Lin, and Ming Chang. 2018. "Optimal Duct Layout for HVAC Using Topology Optimization." *Science and Technology for the Built Environment* 24 (3): 212–19. <https://doi.org/10.1080/23744731.2017.1346444>.
- Perumal, Kumar, and Rajamohan Ganesan. 2016. "CFD Modeling for the Estimation of Pressure Loss Coefficients of Pipe Fittings: An Undergraduate Project." *Computer Applications in Engineering Education* 24 (2): 180–85. <https://doi.org/10.1002/cae.21695>.
- Raber, E., A. Jin, K. Noonan, R. McGuire, and R. D. Kirvel. 2001. "Decontamination Issues for Chemical and Biological Warfare Agents: How Clean Is Clean Enough?" *International Journal of Environmental Health Research* 11 (2): 128–48. <https://doi.org/10.1080/09603120020047519>.
- Reed, Nicholas G. 2010. "The History of Ultraviolet Germicidal Irradiation for Air Disinfection." *Public Health Reports* 125 (1): 15–27. <https://doi.org/10.1177/003335491012500105>.
- Röhrig, R., S. Jakirlić, and C. Tropea. 2015. "Comparative Computational Study of Turbulent Flow in a 90° Pipe Elbow." *International Journal of Heat and Fluid Flow* 55: 120–31. <https://doi.org/10.1016/j.ijheatfluidflow.2015.07.011>.
- Salehi, Mohammad, Ahmad K. Sleiti, and Stephen Idem. 2017. "Study to Identify Computational Fluid Dynamics Models for Use in Determining HVAC Duct Fitting Loss Coefficients." *Science and Technology for the Built Environment* 23 (1): 181–91. <https://doi.org/10.1080/23744731.2016.1204889>.
- Sleiti, Ahmad, Mohammad Salehi, and Stephen Idem. 2017. "Detailed Velocity Profiles in Close-Coupled Elbows—Measurements and Computational Fluid Dynamics Predictions (RP-1682)." *Science and Technology for the Built Environment* 23 (8): 1212–23. <https://doi.org/10.1080/23744731.2017.1285176>.
- Smith, Richard D. 2006. "Responding to Global Infectious Disease Outbreaks: Lessons from SARS on the Role of Risk Perception, Communication and Management." *Social Science and Medicine* 63 (12): 3113–23. <https://doi.org/10.1016/j.socscimed.2006.08.004>.
- Snelling, William J., Arsalan Afkhami, Hannah L. Turkington, Claire Carlisle, S. Louise Cosby, Jeremy W.J. Hamilton, Nigel G. Ternan, and Patrick S.M. Dunlop. 2022. "Efficacy of Single Pass UVC Air Treatment for the Inactivation of Coronavirus, MS2 Coliphage and Staphylococcus

Aureus Bioaerosols.” *Journal of Aerosol Science* 164 (February): 106003. <https://doi.org/10.1016/j.jaerosci.2022.106003>.

Wang, Ming Dong, and Ann Margaret Jolly. 2004. “Changing Virulence of the SARS Virus: The Epidemiological Evidence.” *Bulletin of the World Health Organization* 82 (7): 547–48.

Wang, Zhou, Wang Qiang, and Hu Ke. 2020. “A Handbook of 2019-NCoV Pneumonia Control and Prevention.” Hubei Science and Technology Press, 1–108.

Wojewodka, Michael M., Craig White, Shahrokh Shahpar, and Konstantinos Kontis. 2018. “A Review of Flow Control Techniques and Optimisation in S-Shaped Ducts.” *International Journal of Heat and Fluid Flow* 74 (June): 223–35. <https://doi.org/10.1016/j.ijheatfluidflow.2018.06.016>.

Yang, Yi, Alvin C.K. Lai, R. Y.C. Kong, and Qihong Deng. 2017. “Experimental and Numerical Study of the Performance of Upper-Room Ultraviolet Germicidal Irradiation with the Effective Z-Value of Airborne Bacteria.” *Aerosol Science and Technology* 51 (10): 1123–34. <https://doi.org/10.1080/02786826.2017.1334108>.

Zhang, Huihui, Xin Jin, Sunday Segbenu Nunayon, and Alvin C.K. Lai. 2020. “Disinfection by In-Duct Ultraviolet Lamps under Different Environmental Conditions in Turbulent Airflows.” *Indoor Air* 30 (3): 500–511. <https://doi.org/10.1111/ina.12642>.

Experimental Analysis of Fluid Flow in the Chamber Mobile Robot Disinfectant Using Ultraviolet C (UVC)

Moh. Fajri Sidik^{1, a)}, Andi Amijoyo Mochtar^{2, b)}, Nasaruddin Salam^{3, b)}

Author Affiliations

¹*Graduate School of Mechanical Engineering, Gowa, Hasanuddin University, Indonesia, 92171.*

^{2,3}*Department of Mechanical Engineering, Gowa, Hasanuddin University, Indonesia, 92171.*

Author Emails.

^{a)}*First author: fajrisidik.dt@gmail.com*

^{b)}*Corresponding author: andijoyo@unhas.ac.id*

Abstract. Tuberculosis, measles and influenza are diseases that can spread through the air, so the use of additional air cleaning devices such as HEPA filters helps, but these filters require regular maintenance and are not suitable for dusty environments such as in India. Alternatives such as ultraviolet C (UVC) light and air ionisation with self-cleaning filters are being pursued. UVC light with a wavelength of 220-280 nm is effective in inactivating pathogens, and air disinfection with UVC lamps in a 'box' can serve as a standalone air purifier. However, these devices face the challenge of achieving sufficient pathogen residence time in the UVC chamber while maintaining efficient airflow. Previous studies have shown that the addition of baffles in UV chambers can increase exposure time and pathogen deactivation effectiveness, but can affect flow resistance and pressure drop. A decrease in pressure influences energy usage, making it essential to conduct experimental and numerical studies to understand the fluid flow dynamics in UV chambers with different numbers of baffles. This study found that the air flow velocity in the chamber increases with increasing voltage, but decreases with increasing number of baffles in the chamber (N = 0, N = 2, N = 4, N = 6) due to increasing friction and resistance. At 220 volts, the air velocity dropped from 13.16 m/s (N=0) to 11.64 m/s (N=6). At a velocity of 8.5 m/s, the pressure drops from 64 Pa (N=0) to 98 Pa (N=6), and at a velocity of 10.5 m/s, the pressure drops from 102 Pa (N=0) to 143 Pa (N=6) so the addition of baffles increases the pressure drop and reduces the airflow velocity, especially at higher voltages and velocities.

INTRODUCTIONS

Measles, tuberculosis, and influenza are diseases that are known to be airborne [1]–[3]. People with these diseases can be highly contagious and may spread large numbers of viral and bacterial particles through respiratory aerosols. The presence of pathogens released when coughing, sneezing, talking and breathing is strongly influenced by the initial size of the respiratory particles released [4]. Respiratory pathogens released in large droplets (>100 microns) tend to travel ballistically and can hit people in the face or food. [5] At close range (<2 m), social distancing and the use of protection can significantly reduce the risk of transmission [6]. However, respiratory pathogens released in smaller droplets (<100 microns) can spread further. These droplets quickly evaporate into aerosols less than 20 microns in size [7], that remains in the air [8], [9] and potentially infect people over longer distances. These fine aerosols can also spread through poorly maintained mechanical ventilation and air conditioning systems, which can recirculate the air and potentially spread airborne diseases [10].

Given the common threat posed by airborne diseases, the provision of adequate room ventilation is essential to reduce the number of airborne pathogens [6], [8], especially in rooms where many people tend to gather [11]. However, this is not always possible as many rooms have poor design and inadequate ventilation systems, making it difficult to upgrade. In addition, extreme weather conditions (both hot and cold) may prevent the opening of windows or the full use of 'fresh air' mechanical ventilation, which negatively impacts energy consumption and occupant comfort.

In scenarios like this, the use of additional air cleaning devices, such as high-efficiency particulate air (HEPA) filters, can help [12]. HEPA filters are designed to capture very small particles with an efficiency rate of 99.95%. They can be installed inside heating, ventilation and air conditioning (HVAC) systems. This means that HEPA filters can help filter out dust, air pollutants, and even very small particles such as bacteria and viruses, improving the air quality in the rooms connected to the HVAC system [6] or In a self-contained air cleaning device installed indoors, air

from the room is sucked in by a fan, then airborne particles are captured before clean air is blown back into the room [12]. However, HEPA filters need frequent maintenance and replacement, making them unsuitable for dry and dusty environments like those in India, where they can easily become clogged. Accumulated dust and particles on HEPA filters result in high airflow resistance, increasing energy consumption and reducing the clean air delivery rate (CADR). Consequently, alternative technologies such as ultraviolet-C light (UVC) and air ionization with self-cleaning filter technology, which do not face these issues, are being explored.

UVC light with a wavelength of 220-280 nm is known to damage the genetic material (DNA or RNA) of pathogens (viruses or bacteria), thereby preventing them from causing infections [3]. At this wavelength, light photons break hydrogen bonds in nucleic materials, forming pyrimidine dimers, which prevent the genetic replication of pathogens. [13]. Air disinfection using UV light has been applied since the 1930s to reduce the spread of tuberculosis, with open UVC lamps emitting light above the heads of room occupants which is generally the preferred configuration [6].

Air disinfection can also be achieved by installing a UVC lamp inside a 'box' equipped with a fan. This setup can function as a standalone air purifier that is safe to use in a room or within the ductwork of a mechanical ventilation system [14]. The design is similar to a HEPA filter, but the UVC chamber replaces the HEPA filter in this configuration. UVC-based cleaners are more compact and avoid the risk of damage to eyes and skin [15], [16]. The device with UVC light shielded in the box is suitable for use in households, small businesses, and in rural areas to keep the air clean.

However, devices 'UV in a box' face significant technological challenges due to the difficulty of achieving sufficient residence time for pathogens to be inactivated within the UVC chamber, while maintaining reasonable airflow rates at an acceptable financial cost and power consumption. This major challenge can reduce the effectiveness of the device as an infection control measure. Many people mistakenly believe that the device protects occupants from airborne infections, assuming it achieves a disinfection rate of 99.9% based on a 'single-pass' microbiological test. However, such claims can be misleading as they only apply to the air passing through the UV device and do not reflect the overall effect the device has on the room. The design of the device is primarily influenced by the flow rate of the disinfected air supplied to the room (CAD) [17].

In the research [5] with a portable UVC air treatment device with the use of 3 baffles in the UV chamber with an air flow of 1254 L/min can increase the exposure time so as to effectively inactivate bioaerosols containing bacterial and viral indicator organisms, as well as coronaviruses without relying on filtration technology.

However, the addition of baffles can also affect fluid flow and pressure drop in the UV chamber. Pressure drop is one of the influential factors in improving energy utilization, saving energy, and reducing emissions. Experimental and numerical research using CFD to be carried out for the prediction of pressure drop in duct fittings and factors affecting its accuracy [18]–[22].

Seeing the lack of published literature related to fluid flow and pressure drop in the UV chamber, it is necessary to conduct further research to determine the fluid flow characteristics in the UV chamber with the addition of variations in the number of bulkheads and their effect on pressure drop.

METHODS

This research uses an experimental method, the chamber used looks like Figure 1 with dimensions of 54 cm long, 54 cm wide, and 32 cm high.

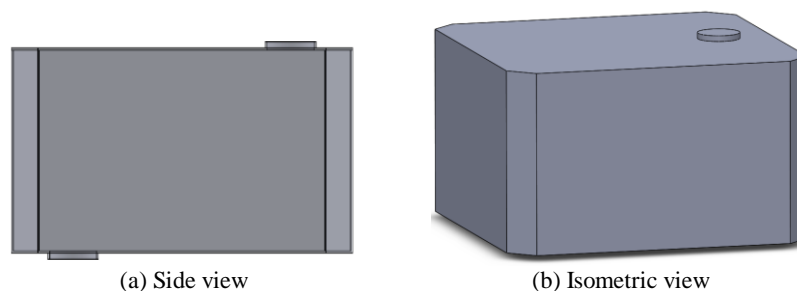


FIGURE 1. Chamber mobile robot UV disinfectant

The inside of the chamber is given a bulkhead with a variation in the number of bulkheads (N) of 0, 2, 4, 6 as shown in Figure 2, Model (a) is a chamber without the addition of bulkheads ($N = 0$),

model (b) added 2 bulkheads with a distance between bulkheads of 103 mm ($N = 2$), in model (c) added 4 bulkheads with a distance between bulkheads of 65 mm ($N = 4$), and in model (d) added 6 bulkheads with a distance between bulkheads of 52 mm ($N = 6$).

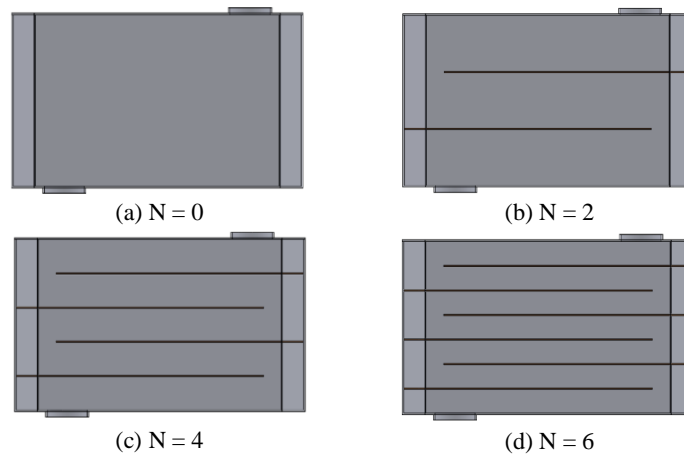


FIGURE 2. Number of baffles in the chamber, showing (a) Without baffles, (b) Two baffles, (c) three baffles, (d) Four baffles.

The research installation is in the form of a test section with ACP (aluminum composite panel) material and bulkhead using inpraboard material. Measuring instruments using pitot tube and pressure tap with V manometer of kerosene fluid to measure static pressure and dynamic pressure. The scheme of the testing equipment looks like Figure 3.

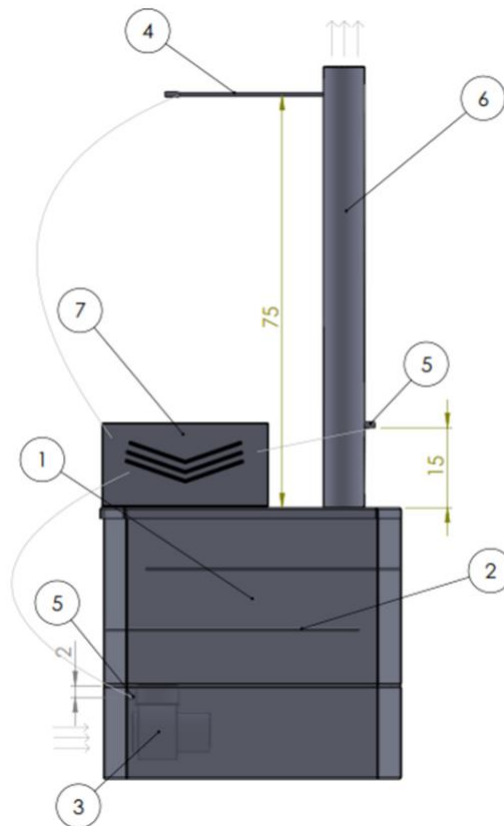


FIGURE 3. Testing scheme of the disinfectant mobile robot chamber

The test setup for UV disinfection, as depicted in the diagram, features a test chamber (1) designed for UV disinfection. Inside the chamber, bulkheads (2) are placed to direct and control the airflow. A centrifugal blower (3) is used to circulate air through the system. The airflow velocity is measured using a pitot tube (4), while pressure differences are monitored via pressure taps (5). To ensure stable airflow, a flow conditioning pipe (6) is included. Additionally, a V manometer (7) is utilized to track pressure readings accurately.

Experimental testing was carried out 4 times, the first test was carried out without the addition of bulkheads ($N = 0$), the second using 2 bulkheads ($N = 2$), the third using 4 bulkheads ($N = 4$), and the fourth using 6 bulkheads ($N = 6$).

The testing procedure with an experimental approach is the first step in this test is to prepare the tools and materials to be used. After that, the chamber is made according to the design in the predetermined computational method. Then, the installation of test installation tools is carried out, including blowers, pressure taps, and pitot tubes. The blower was activated and the voltage was set at 100 volts. After the blower turns on, pressure data is taken at the pressure tap and pitot tube after waiting for 3 minutes so that the fluid flow is more stable, so that the data obtained is more accurate. The step of activating the blower and adjusting the voltage, as well as taking this data was repeated at voltages of 130 volts, 160 volts, 190 volts, and 220 volts. Following that, the test proceeded by adding bulkheads to the chamber, starting with 2 bulkheads, then 4 bulkheads, and 6 bulkheads, maintaining the same procedure for each different bulkhead configuration.

Data processing begins with an example calculation involving some initial data. First, the inclined manometer angle (θ) used in the calculation is 15° . Next, the Specific Gravity of kerosene (SG_{kerosene}) of 824 kg/m^3 is required to calculate the specific gravity of kerosene. The acceleration of gravity (g) used was 9.81 m/s^2 , which is a standard value in gravity calculations. The room temperature is considered constant at 28°C (T), while the density of air at that temperature (ρ_{Air}) is 1.182 kg/m^3 . Finally, the density of water at 28°C ($\rho_{\text{H}_2\text{O}}$) is 996.4 kg/m^3 . These data are essential in determining the parameters and variables required in the calculation process. The velocity calculation is measured on the flow conditioning pipe using a pitot tube. The fluid velocity calculation is written according to equation 1.

$$v = \sqrt{\frac{2 \cdot (p_0 - p_s)}{\rho_{\text{air}}}} \quad (1)$$

Because it uses a 15° V manometer, it becomes :

$$v = \sqrt{\frac{2 \cdot \rho_{\text{kerosene}} \cdot g \cdot (\Delta h \cdot \sin 15)}{\rho_{\text{air}}}} \quad (2)$$

Where, p_0 is the stagnation pressure measured by the stagnation pressure tube, p_s is the static pressure parallel to the stagnation pressure tube, ρ_{air} is the density of air at 28°C , ρ_{kerosene} is the density of kerosene at 28°C . Dynamic pressure is the difference between stagnation pressure and static pressure ($p_0 - p_s$).

Pressure drop (ΔP) is the difference in inlet pressure and outlet chamber pressure as shown in Figure 3. The calculation of P_{inlet} and P_{outlet} is as follows:

$$\Delta p = p_{\text{inlet}} - p_{\text{outlet}} \quad (3)$$

$$\Delta p = (\rho_{\text{kerosene}} \cdot g \cdot (\Delta h_{\text{inlet}} \cdot \sin 15)) - (\rho_{\text{kerosene}} \cdot g \cdot (\Delta h_{\text{outlet}} \cdot \sin 15)) \quad (4)$$

Where, Δp is the pressure drop measured in Pascal (Pa), p_{inlet} is the pressure at the inlet chamber also measured in Pascal (Pa), p_{outlet} is the pressure at the outlet chamber in the same unit, and g is the acceleration of gravity measured in metres per second squared (m/s^2).

RESULT AND DISCUSSION

Mechanism Control

The use of a dimmer as a voltage regulator on a centrifugal blower is a method used to control the rotation speed of the blower motor, so that the air flow produced can be adjusted as needed. Dimmer works by adjusting the amount of voltage applied to the blower motor. The test results of dimmer power variations on fluid velocity in each bulkhead can be seen in Figure 4.

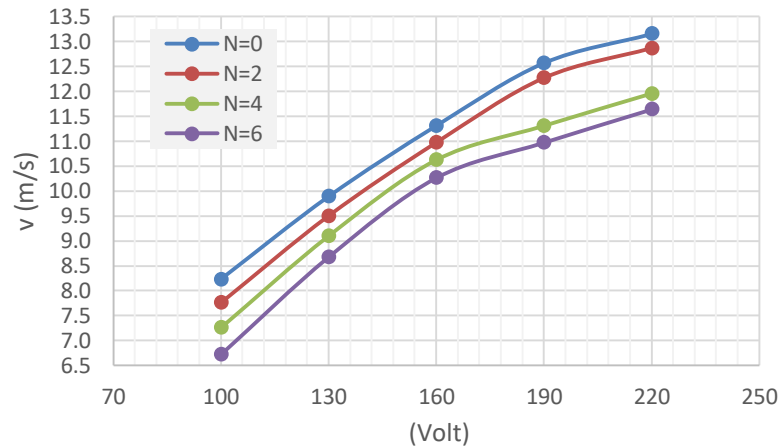


FIGURE 4. Comparison between voltage power and airflow velocity

The graph in Figure 4 shows the comparison between voltage power (Volt) and airflow velocity (v in m/s) on the centrifugal blower for various number of baffles ($N = 0, N = 2, N = 4, N = 6$). It can be seen that the airflow velocity increases as the applied voltage increases, at $N = 0$ the air velocity for a voltage of 100 volts is 8.23 m/s then continues to increase until at a voltage of 220 volts the air velocity is 13.16 m/s. However, increasing the number of baffles (N) in the chamber causes a decrease in airflow velocity at the same voltage. For example, at a voltage of 220 volts, the airflow velocity for $N = 0$ reaches about 13.16 m/s, while for $N = 6$ it is only about 11.64 m/s. The addition of baffles to the chamber causes an increase in friction force and airflow resistance, resulting in a decrease in airflow velocity.

Pressure Drop

Pressure drop in the inlet and outlet chamber areas, obtained graphs as in Figure 5.

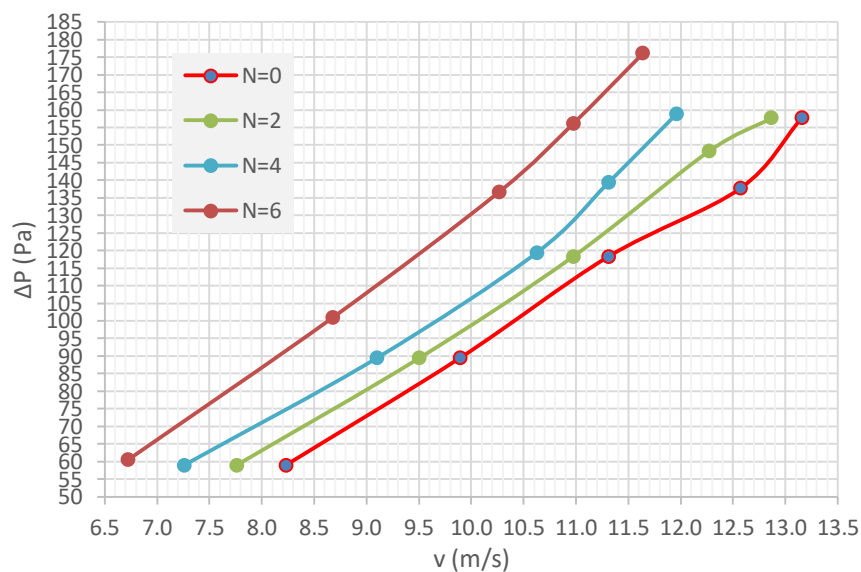


FIGURE 5. Comparison of Speed to Pressure Drop

In Figure 5, it can be seen that there is a difference in speed in each bulkhead variation at the same electrical power. At 100 volts, it can be seen that $N = 0$ produces a speed of 8.23 m/s, $N = 2$ produces a speed of 7.76 m/s, $N = 4$ produces a speed of 7.26 m/s, and $N = 6$ produces a speed of 6.72 m/s. It can be seen that the more the bulkhead increases, the fluid velocity decreases, the difference in speed occurs due to differences in surface friction in each variation resulting in a decrease in speed as the bulkhead increases and the speed increases with increasing electrical power.

To be able to see the value of the pressure drop at the same speed for each variation in the number of bulkheads we can draw a straight line at 5 speeds on the graph in Figure 5 so that a graph like Figure 6 is obtained.

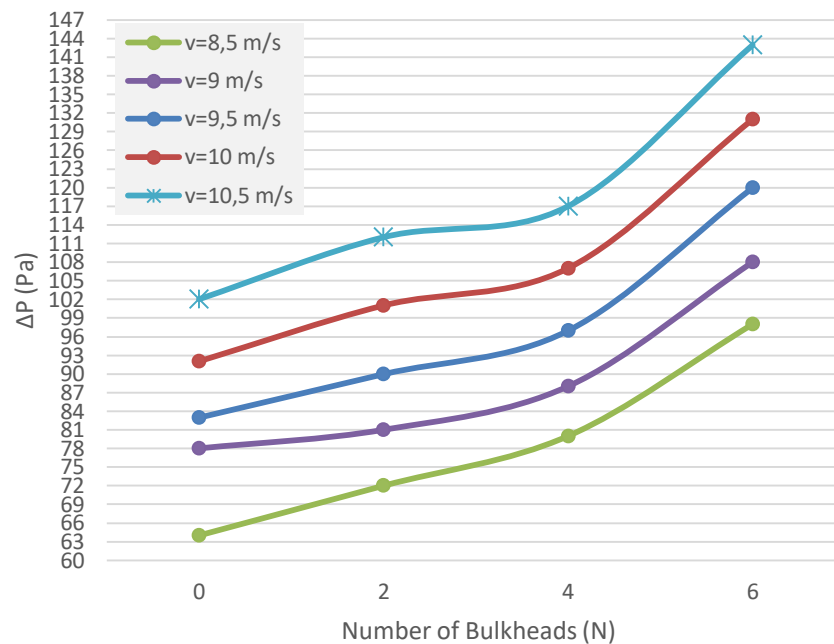


FIGURE 6. Comparison of Pressure Drop Against Number of Bulkheads

From Figure 6 it can be seen that at a speed of 8.5 m/s the chamber without bulkheads produces the lowest pressure drop value with a value of 64 Pa, then increases with the addition of 2 bulkheads with a value of 72 Pa, 4 bulkheads with a value of 80 Pa, and the highest pressure drop is in the chamber with the addition of 6 bulkheads with a value of 98 Pa. So, with the addition of bulkheads in the chamber, the value of the pressure drop increases and the increase that occurs is getting higher as the number of bulkheads increases. It can also be seen that the pressure drop that occurs increases with increasing speed where at a speed of 10.5 m/s the value of the pressure drop in the chamber without bulkheads is 102 Pa, 2 bulkheads with a value of 112 Pa, 4 bulkheads with a value of 117 Pa, and at 6 bulkheads with a value of 143 Pa.

CONCLUSION

Experimental analysis of fluid flow in the chamber of the mobile robot uv disinfectant was carried out to determine the flow characteristics and pressure drop, showing that the air flow velocity in the chamber increases with increasing voltage, but decreases with increasing number of baffles in the chamber ($N = 0$, $N = 2$, $N = 4$, $N = 6$) due to increasing friction and resistance. At 220 volts, the air velocity drops from 13.16 m/s ($N = 0$) to 11.64 m/s ($N = 6$). In addition, the addition of baffles also caused an increase in pressure drop, at 8.5 m/s, the pressure dropped from 64 Pa ($N = 0$) to 98 Pa ($N = 6$). at 9.5 m/s, the pressure drops from 83 Pa ($N = 0$) to 120 Pa and At 10.5 m/s, the pressure drops even higher from 102 Pa ($N = 0$) to 143 Pa ($N = 6$). This shows that the addition of bulkheads significantly increases the pressure drop and decreases the airflow velocity, especially at higher stresses and velocities.

ACKNOWLEDGMENTS

Institute for Research and Community Service (LPPM) Hasanuddin University. Number: 1474/UN4.22/PT.01.03/2022.

REVERENCE

1. F. Yang, Z. Li, Y. Yuan, C. Liu, Y. Zhang, and Y. Jin ‘Numerical and Experimental Investigation of Internal Flow Characteristics and Pressure Fluctuation in Inlet Passage of Axial Flow Pump under Deflection Flow Conditions’, *Energies*, 14.17 (2021).
2. T. Greenhalgh, J. L. Jimenez, K. A. Prather, Z. Tufekci, D. Fisman, and R. Schooley, ‘Ten Scientific Reasons in Support of Airborne Transmission of SARS-CoV-2’, *The Lancet*, 397.10285 (2021), 1603–5.
3. C. B. Beggs and E. J. Avital, ‘Upper-Room Ultraviolet Air Disinfection Might Help to Reduce COVID-19 Transmission in Buildings: A Feasibility Study’, *PeerJ*, 8 (2020), e10196 “Upper-room ultraviolet air disinfection might help to reduce COVID-19 transmission in buildings: A feasibility study,” *PeerJ*, vol. 8, p. e10196, Oct. (2020).
4. C. B. Beggs and E. J. Avital, ‘A Psychrometric Model to Assess the Biological Decay of the SARS-CoV-2 Virus in Aerosols’, *PeerJ*, 9 (2021), e11024.
5. W. J. Snelling *et al.*, ‘Efficacy of Single Pass UVC Air Treatment for the Inactivation of Coronavirus, MS2 Coliphage and Staphylococcus Aureus Bioaerosols’, *Journal of Aerosol Science*, 164. February (2022), 106003.
6. L. Morawska *et al.*, ‘How Can Airborne Transmission of COVID-19 Indoors Be Minimised?’, *Environment International*, 142 (2020), 105832.
7. X. Xie, Y. Li, A. T. Y. Chwang, P. L. Ho, and W. H. Seto, ‘How Far Droplets Can Move in Indoor Environments – Revisiting the Wells Evaporation–Falling Curve’, *Indoor Air*, 17.3 (2007), 211–25.
8. G. Seminara, B. Carli, G. Forni, S. Fuzzi, A. Mazzino, and A. Rinaldo, ‘Biological Fluid Dynamics of Airborne COVID-19 Infection’, *Rendiconti Lincei*, 31.3 (2020), 505–37.
9. V. Stadnytskyi, C. E. Bax, A. Bax, and P. Anfinrud, ‘The Airborne Lifetime of Small Speech Droplets and Their Potential Importance in SARS-CoV-2 Transmission’, *Proceedings of the National Academy of Sciences of the United States of America*, 117.22 (2020), 11875–77.
10. L. Anghel *et al.*, ‘Impact of Hvac-Systems on the Dispersion of Infectious Aerosols in a Cardiac Intensive Care Unit’, *International Journal of Environmental Research and Public Health*, 17.18 (2020), 1–17.
11. C. B. Beggs, S. J. Shepherd, and K. G. Kerr, ‘Potential for Airborne Transmission of Infection in the Waiting Areas of Healthcare Premises: Stochastic Analysis Using a Monte Carlo Model’, *BMC Infectious Diseases*, 10.1 (2010), 1–8.
12. M. J. Butler *et al.*, ‘Impact of Supplementary Air Filtration on Aerosols and Particulate Matter in a UK Hospital Ward: A Case Study’, *Journal of Hospital Infection*, 135 (2023), 81–89.
13. C. B. Beggs, ‘A Quantitative Method for Evaluating the Photoreactivation of Ultraviolet Damaged Microorganisms’, *Photochemical and Photobiological Sciences*, 1.6 (2002), 431–37.
14. Y. Qiao *et al.*, ‘Greater than 3-Log Reduction in Viable Coronavirus Aerosol Concentration in Ducted Ultraviolet-C (UV-C) Systems’, *Environmental Science and Technology*, 55.7 (2021), 4174–82.
15. A. P. Cullen, ‘Photokeratitis and Other Phototoxic Effects on the Cornea and Conjunctiva’, *International Journal of Toxicology*, 21.6 (2002), 455–64.
16. G. I. Harrison and A. R. Young, ‘Ultraviolet Radiation-Induced Erythema in Human Skin’, *Methods*, 28.1 (2002), 14–19.
17. H. C. Burridge *et al.*, ‘The Ventilation of Buildings and Other Mitigating Measures for COVID-19: A Focus on Wintertime’, *Proceedings of the Royal Society A*, 477.2247 (2021).
18. K. Perumal and R. Ganesan, ‘CFD Modeling for the Estimation of Pressure Loss Coefficients of Pipe Fittings: An Undergraduate Project’, *Computer Applications in Engineering Education*, 24.2 (2016), 180–85.
19. R. Röhrig, S. Jakirlić, and C. Tropea, ‘Comparative Computational Study of Turbulent Flow in a 90° Pipe Elbow’, *International Journal of Heat and Fluid Flow*, 55 (2015), 120–31.

20. Salehi, Mohammad, Ahmad K. Sleiti, and Stephen Idem, 'Study to Identify Computational Fluid Dynamics Models for Use in Determining HVAC Duct Fitting Loss Coefficients', *Science and Technology for the Built Environment*, 23.1 (2017), 181–91.
21. A. Sleiti, M. Salehi, and S. Idem, 'Detailed Velocity Profiles in Close-Coupled Elbows—Measurements and Computational Fluid Dynamics Predictions (RP-1682)', *Science and Technology for the Built Environment*, 23.8 (2017), 1212–23.
22. I. Malanichev and F. Akhmadiev, 'Pressure Loss Reduction in Ventilation Ducts by Shape Optimization of the Removable Profiled Components', *IOP Conference Series: Materials Science and Engineering*, 890.1 (2020).